Delft University of Technology

Hydraulic Engineering MSc Thesis

Wave Loads on Emerged Breakwater Crown Walls, a Physical Model Study

Author:
Martijn Veringa (5159768)

Committee:	Dr. ir. Bas Hofland	TU Delft (Chair)
	Prof. dr. ir. Marcel R.A. van Gent	TU Delft & Deltares
	Dr. ir. Alessandro Antonini	TU Delft
	Ir. Dennis C.P. van Kester	Van Oord & TU Delft
	Ir. Gregory Smith	Van Oord

May 25, 2023

TU Delft Delft University of Technology

TKI DELTATECHNOLOGIE

Van Oord Marine ingenuity

Abstract

This study investigates the loading characteristics of breakwater crown walls, which are large permeable structures that are mainly constructed using rock. Crown walls are typically added to conventional breakwaters to reduce the total rock volume required for construction, provide access to the breakwater, and reduce overtopping rates. However, there is still uncertainty regarding the estimation of uplift pressures and a time delay between the maximum horizontal forces on the wall face and the maximum vertical force on the underside of the crown wall. The objective of this study is to identify and analyze the governing parameters of the pressure distribution and total force on the underside of the crown wall, and to understand the presence of time lags between maximum horizontal and vertical maximum forces and its role in stability and design of crown walls. In this study specifically in the influence of the foundation level was investigated

To achieve this objective, physical scale-model tests were conducted at the Hydraulic Engineering Laboratory of the University of Delft. The model is a 1:1.9 slope rouble mound breakwater, with a 2 d_{n50} thick armour layer, which is fixed along with the wide graded core. Twelve temperature shock proof pressure sensors are used along the base and face of the crown wall, which has a protected and unprotected part. The study varied a number of parameters, such as wave height ($H_s \sim$ 0.125-0.175m), steepness ($s \sim$ 0.015-0.040), foundation level (F_c/H_s $\sim$ 0-0.5), armour crest width($Gc/d_{a,n50} \sim$ 2.5-4), and crown wall height ($h_c/H_s \sim$ 0.6-1.6), and investigated their influence on wave loading. The time lag between maximum horizontal and vertical pressures was also recorded. Additionally, the overall stability of a model crown wall under varying wave conditions and geometrical set-ups was tested. By iteration, a minimal weight of non-failure of the crown wall can be found for a given wave condition. These results are used to introduce a new method of analysis based on the instance of lowest factor of safety, or minimum stability.

The results of this study show that the conventional design methods based on a triangular pressure distribution are accurate but incomplete. This shape does not accurately represent non-zero foundation levels. The study also reports a relative time lag ($\Delta t/T_p$) between horizontal and vertical maximum pressures in the range of 0-0.2 [-], which must be considered in stability considerations for non-zero foundation level wave conditions. For this a reduction factor on the vertical loading for stability calculations is introduced, namely $\gamma_t = \frac{F_{V,0.1\%,FoS}}{F_{V,0.1\%,max}} = -1.52\frac{F_c}{H_s} + 1.0$. Furthermore, the influence of various parameters on vertical loading, such as wave height, steepness, foundation level, and armour crest width, is investigated, and their correlation with vertical forces is revealed. The importance of taking foundation level and armour crest width into consideration is highlighted. The proposal to use overtopping as a force estimator is rejected.

Preface

I was able to complete this thesis and write this report because of the genuine support and help of others. I'd like to thank my parents, brother, sister, girlfriend and friends. I'd like to thank my committee for their feedback and time and Dennis in particular for his excellent support throughout this past year. I'd also like to thank the Coastal Engineering department at Van Oord for welcoming me into their team. Finally, I'd like to thank the wonderful team of the Hydraulic Lab at the TU Delft for their efforts to make my experiments a success. It's been a long process with a rocky ending to it, but I'm glad with what I've got to show for it and hope you enjoy reading about it.

Contents

1 Introduction

Wave action is an important problem encountered by ports and vessels as calm wave conditions are a must for safe entry, exit and mooring in ports. These calm conditions can only be generated by structures that shelters the port and access channels from large waves. This is the main purpose for which breakwaters are constructed. Figure 1 shows this calmer wave climate within the bounds of the numerous breakwaters of the port of Hanstholm, Denmark.

Figure 1: Protected calm waters in the port basin and access channel of Hanstholm port (Group, n.d.).

Conventional breakwaters are large permeable structures that are mainly constructed using rock. A typical adaptation to a conventional breakwater is the addition of a crown wall. In figure 2, such a crown wall and its impact on the cross section are visualised. A conventional breakwater consists of a rock core, a filter and an armour layer on which the waves break. Figure 2 also illustrates clear advantages of crown walls, as opposed to a conventional design. Firstly, the total rock volume that is necessary for the construction is decreased. Also, it provides access to the breakwater, with its flat concrete surface. This can be used for maintenance and recreation, but also pipelines and other installations can be built over the full length of the breakwater. With a crown wall that extends above the armour crest level, overtopping rates can be greatly reduced as the impermeable wall face reflects much of the run-up.

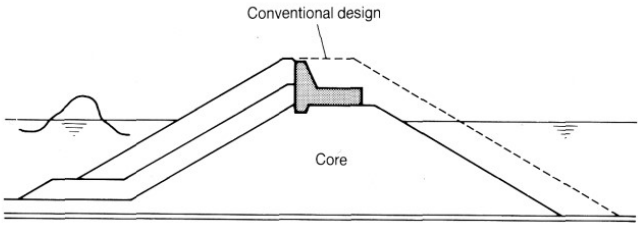

Figure 2: Difference in geometry between conventional rubble mound breakwater and one with a crown wall (CIRIA, 2007).

1.1 Relevancy and motivation

Over the last 40 years some important steps have been taken to better understand wave-structure interaction for a crown wall. However, recent model tests by Van Oord and academics (Molines et al. (2018), Negro Valdecantos et al. (2013)) have shown that different methods show a large discrepancy in results and that often design methods overestimate the wave loads on the structure. This indicates a possible inadequate understanding of the wave-structure interaction and of the relevant parameters and their relative influence. Both from an academic and design perspective this encourages more research on the matter.

A better design method supported by better understanding as outlined before, can contribute

to more realistic and reliable crown wall designs. This would be mainly the consequence of less concrete being used, which in turn lowers the CO2 footprint of the construction (Fennell et al., 2021). From the academic perspective, better understanding of the interactions is also encouraged. The confidence that a better understanding could be achieved through more model tests is partly founded on the expectation that new sensors could improve the measurements.

1.2 Problem analysis

In this study, the aforementioned matter of 'a possible inadequate understanding of the wave-structure interaction and of the relevant parameters and their influence' was studied. From the literature a few knowledge gaps were identified, which this study aims to fill in.

Uplift pressure

The maximum horizontal force that wave loads exert on crown walls is fairly well understood and described by numerous methods (Negro Valdecantos et al., 2013) (Molines & Medina, 2019). The biggest uncertainty and spread in results comes from estimations of uplift pressures. In early scale model tests these pressures were not even measured, like in the influential work by Pedersen (1996). A common description assumes simultaneous maximum horizontal and vertical loading and relies on a hydrostatic assumption that the horizontal pressure at its toe of the crown wall is the same as the uplift pressure at the toe. The rest of the distribution is then considered linear and decreasing to zero at the heel of the wall. From this basic model some adaptations have been proposed. Martin et al. (1999) proposed to replace the assumption of zero pressure at the heel, for a value of possibly non-zero value p_{re}, which is a function of the crown base width and wavelength. Losada & Dalrymple (1993) formulated a parabolic distribution, instead of the linear one, by applying linear wave theory. Bekker et al. (2018) more closely focussed on uplift pressures and found that the distribution was S-shaped and hyperbolic for large freeboard (grey pressure distribution in figure 3). Moreover, Bekker suggested that - unlike Martin's suggestion that the pressure could be non-zero at the heel - the pressure can drop to zero even halfway the underside of the crown wall, introducing the reduction factor γ_v (a function of x_c in figure 3).

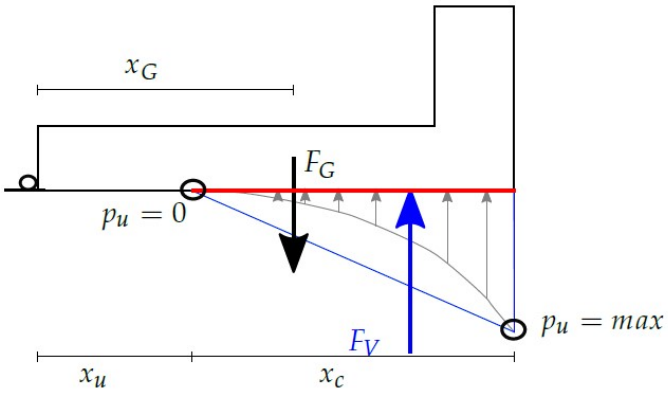

Figure 3: Vertical forces and pressures working on a crown wall as proposed by Bekker (Bekker et al., 2018).

The relation of uplift to different parameters is also not well understood. Martin et al. (1999) method attempts to include crown wall width and core porosity, based on numerical simulation by Losada & Dalrymple (1993), but no actual model tests were done. Concerning the armour crest width: authors often do mention the number of units or rocks on the armour crest but

have not formulated a clear dependence between this armour crest width and the loading of the crown wall. It is expected that this parameter influences the load reduction on the sheltered part of the wall face, but the direct relation is unclear. This reduced load is in many methods the basis for the determination of the uplift pressure distribution, so the armour crest width is expected to influence the uplift (estimation) too. Also, more generally a longer distance to the wall is expected to influence the uplift pressure (distribution). Concerning the freeboard level of the crown wall (relative to SWL), Bekker et al. (2018) extended existing methods by Pedersen (1996) and Nørgaard et al. (2013) to have better results for increasing freeboard. Bekker et al. (2018) mentions, however, that due to the heavy filtering of the data, its predictions may be unreliable.

Time lag

Another phenomenon that has been observed but is not yet fully understood, is the issue of a time delay between the highest pressures on the wall face and the highest pressures on the underside of the crown wall. This has been illustrated by Nørgaard et al. (2013) by showing the lack of correlation between the maximum uplift pressures and the uplift pressures simultaneous with the maximum horizontal pressures. These time lags are also illustrated quite clearly by Franco et al. (2018) and Aniel-Quiroga et al. (2019), but no physical explanations or proposed methods are connected to these findings. Figure 4 shows these time lags. In the top figure the temporal pressure distribution for three different sensors on the fully protected vertical wall face is shown. The lower one shows the temporal pressure distribution for three sensors on the wall base.

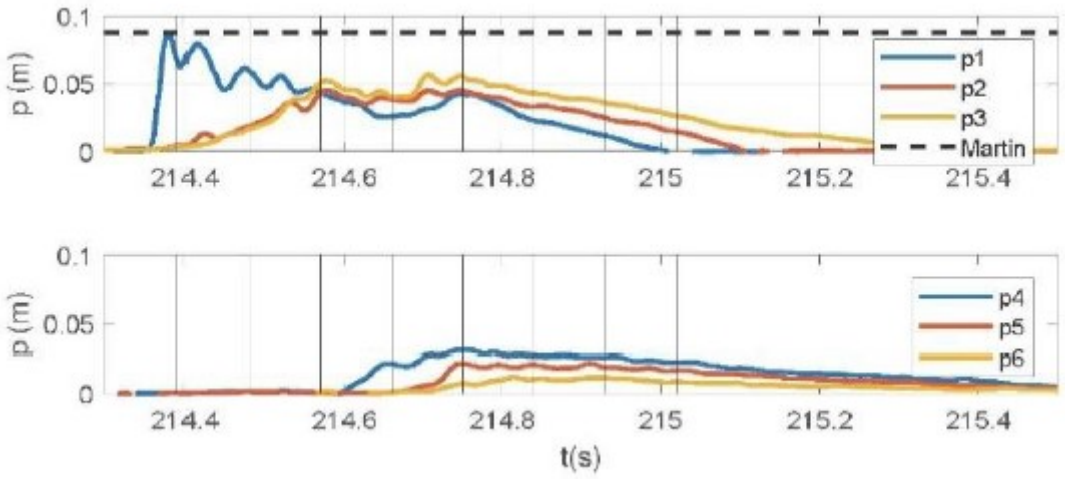

Figure 4: Temporal distribution of pressures on a crown wall. Top panel shows the horizontal pressures for three different points on the front face (from p1 at the top and p3 at the bottom). Bottom panel shows the vertical pressure on the underside for the same wave on different locations (from p4 at the front and p6 at the rear)(Franco et al., 2018).

Overtopping

In light of a recent analysis and introduction of overtopping as governing parameter in wave load predictions by Molines et al. (2018), overtopping will also be considered in this study. Molines et al. (2018) argue that since virtual run-up (which is the basis of many contemporary methods) cannot be measured, it is unfit to be used as a key variable in the analysis. Overtopping is the suggested replacement of virtual run-up and introduced as a reasonable explanatory variable. The

conclusions from Molines et al. (2018) include that their method predict the loads on the crown wall similarly but using more simple formulations. The existence of a correlation between these wave forces and overtopping was also independently tested and analysed (Franco et al., 2018), (Cecioni et al., 2019). Although similar conclusions to Molines et al. (2018) are drawn, both papers state the high degree of variability in the results.

1.3 Objective

This study aims to fill in (parts of) the knowledge gap that is described in the previous section. In a general sense the question this study aims to answer is:

> *Can current design methods for force estimations on crown walls be improved in their description of relevant phenomena and relation between wave conditions and horizontal and vertical forces on crown walls?*

To guide the answering of this research question, some sub-questions are formulated, namely:

- *How can uplift pressure distributions be described?*
- *What parameters are governing in estimating uplift pressures?*
- *Do time lags between horizontal and vertical maximum pressures occur and how can they be included in a design method?*
- *Can the use of estimates of wave overtopping improve estimates of wave loads?*

1.4 Methodology

The approach to this study consists of three parts: literature review, physical testing and data analysis of the tests. These three sections also form the core of this report, each with its own chapter.

Literature Review

In order to fully understand the context of crown wall stability on rubble mound breakwaters a literature review was conducted. This also served to better understand the knowledge gap for this topic to further steer the objectives of this study. Finally, the review laid the ground work for the design of the physical model tests, for both the set-up and the model conditions. The review consists of two parts: an overview of some of the relevant concepts in the design and construction of rubble mound breakwaters and crown walls and a second (more in depth) part that details the most prevalent design methods for breakwaters and specifically crown walls. These different methods are described, critically analysed and compared to one another to give an impression of the state of the art in this field. This forms the basis for the formulation of the knowledge gap.

Model Tests

Using the facilities in the Hydraulic Engineering Laboratory of the University of Delft, physical model tests were performed to help answer the research questions. Using a scaled-down model, real world physical phenomenon (wave impact, sliding failure, overtopping, etc.) were simulated. In these tests a number of parameters were varied, with a focus on - using a representative range of wave conditions - investigating the influence of the foundation level (F_c), armour crest width (G_c) and crown wall height on the wave loading. In addition overtopping rates and the time lag between maximum horizontal and vertical pressures were recorded. Alongside these measurements, the overall stability of a model crown wall under varying wave conditions and geometrical set-ups was tested. By iteration a minimal weight of non-failure of the crown wall can be found for a given wave condition.

Data Analysis

In this final core part the results of the model tests are analysed. First the validity of the tests is analysed, by examining the model set-up and wave conditions. Then, the stability tests are analysed. Then the results of the pressure measurements are presented, which are filtered and calibrated in part using the stability test results. Special attention is given to pressure distribution along the crown wall. Using the pressure signal and extrapolated values, horizontal and vertical forces and the factor of safety are determined. These three factors are analysed for different geometries and hydraulic boundary conditions. Then, the governing parameters for vertical forces are identified and analyse. Finally, the found values are compared to the expected values as per the literature review.

1.5 Reading Guide

2. *Rubble mound breakwaters and crown walls*
   This chapter gives the necessary context to the study that was done. It introduces the function and general geometries of breakwater and expands on this for the special case of rubble mound breakwater with crown walls. It also gives an overview of the loading mechanism, failure modes and stability criteria for crown walls.

3. *Literature Review*
   This chapter gives an overview of the current methods that are described in the literature to estimate wave loads on and design breakwater crown walls. The methods are described, critically analysed and compared to one another to give an impression of the state of the art in this field.

4. *Physical model test set-up*
   In this chapter the details of the small scale physical model that is used to perform the test are covered. Special attention is given to the physical model itself, the test conditions and the measurement apparatus.

5. *Model test results and analysis*
   The results that are considered relevant to the study are described here. This includes the processing of the data signals as well as in depth analysis of the observed phenomena and relations.

6. *Discussion*
   In this chapter a critical analysis of the research findings and limitations of the research are detailed.

7. *Conclusions and recommendations*
   The answer to the research questions and other conclusions are presented in this chapter. This thesis ends with some recommendations for further study.

2 Rubble mound breakwaters and crown walls

2.1 Rubble mound breakwaters

Rubble mound breakwaters are large permeable coastal structures mainly constructed from rock. They primarily dissipate wave energy in a variety of contexts. Most notably, this is done in and around ports to facilitate the safe entry, exit and mooring of vessels in the port. The positioning and cross section design of the breakwater is chosen such that potential large (or for that matter any) waves can only partially penetrate to areas where calm wave conditions are necessary. Breakwaters achieve this goal by dissipating a large part of the wave energy, as waves break on their slopes. Primarily when the objective is to reduce coastal erosion, breakwaters also play a role in limiting the effects of currents.

Breakwater design

There exits a large variety of breakwater geometries. In this section two important geometries are introduced (in figure 5) and important consideration about the crucial elements or a rubble mound breakwater are detailed.

1. *Conventional rubble mound*
   Arguably the most common type of breakwater. It is often built using a large core of quarry run. On top of this initial layer, typically, a filter layer is constructed to prevent the core material from being washed out by wave action or currents. In some cases more filter layers are necessary or geotextiles (in combination with a filter layer) are used. The upper most layer is the armour layer, which is directly exposed to the wave attack and it protects the structure from failure due to the wave loads. Instead of rocks the armour layer can also be designed using heavy concrete elements.

2. *Conventional rubble mound with crown wall*
   An adaptation to the conventional rubble mound is the crown wall. More details about this adaptation are given in the following section.

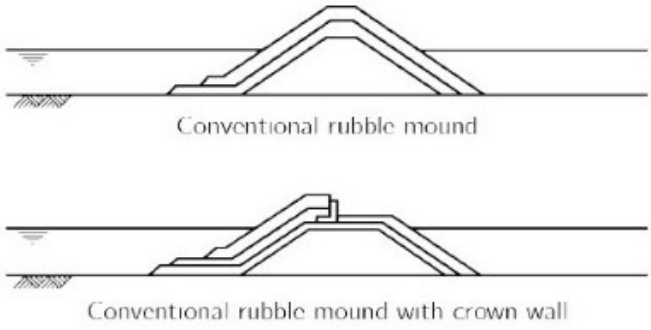

Figure 5: Different configurations of rubble mound breakwaters (adapted from Van den Bos & Verhagen (2018)).

Apart from the choice of configuration many other things need to be considered in the design of a rubble mound breakwater. Here a few crucial ones are expanded on.

Armour

For the design of the armour layer a few important dimensions are the armour stone diameter, the

layer thickness and the width of the armour crest. Typically, the design equations as formulated by Van der Meer (1987) are used for the armour stone diameter, which mainly relates the the nominal diameter of the rock armour to a design wave height. Other important factors that are taken into account are the relative buoyant density of the rocks, the slope angle, the number of incident waves in a storm event and the surf similarity parameter (ξ_m, more on this in 2.2).
The minimal orthogonal thickness of this armour layer is quantified by the following equation:

$$t_{armour} = nk_t D_{n50}, \tag{1}$$

where n is the number of layers (typically 2 for rock armour), k_t is the layer thickness coefficient (typically assumed to be 1) and D_{n50} is the median nominal stone size.

Core

Most of the rock volume in a conventional breakwater is in the core and it is not directly influenced by wave loading and thus cost-effective material is used. For a typical core quarry run is used, which more or less are the left-overs from the quarry's production. One of the few conditions that is put on this material is a limitation on the mass fraction of the finest material in it. A large mass fraction of fines can greatly reduce the permeability of the breakwater, which decreases its resistance to waves as much more energy per wave is dissipated by it.

Filters

Since the core is filled with smaller rocks than the armour, it is at risk of being washed-out. To ensure this does not happen the layers are subject to a stability criterion, which are given in table 1. These criteria ensure *stability, permeability and internal stability* of the filters and are dependent on varying mass fractions of the base (b) or filter (f) layers. Notably, CIRIA (2007) formulates an exception on the permeability criterion for widely graded materials.

Filter rule	Criterion	Exception
Stability	$d_{15f}/d_{85b} < 5$	-
Permeability	$d_{15f}/d_{15b} > 5$	>1 (wide grading)
Internal Stability	$d_{60}/d_{10} < 10$	-

Table 1: Filter rules as given by CIRIA (2007)

2.2 Crown walls

A possible addition to a simple rubble mound breakwater is a crown wall, which is an important part of this research. This addition to the breakwater has a few possible functions. Firstly, it allows easier access to the full length of the breakwater. This could be used for maintenance work and surveying, but also pipelines and other installations can be built over the full length. This access road is also an opportunity for tourists and visitors to walk along the breakwater. A crown wall also reduces overtopping. This could have numerous advantages, like reducing the load on the rear slope which could entail that the slope requires less armour. It also decreases loads on potential vessels stationed or sailing on the lee side of the breakwater. A final advantage is the reduction in necessary quarry material for the construction. The L-shaped crown wall reduces the total rock or block volume (figure 2) and thus the construction costs.

Design

The geometries of crown walls exhibit significant variety, as depicted in Figure 6. Some designs, such as a simple wave screen, rely primarily on the active and passive pressures generated by the breakwater core to maintain stability. In contrast, more common configurations rely on friction with the core or top layer to prevent sliding, or on the wall's weight to prevent overturning. These displacements - which are likely failures of the structure - are discussed in more detail later. Recurved faces or parapents are adaptations focussed on further decreasing overtopping without having to resort to an increase in the wall height. Finally, a penetrating skirt gives the common configuration an additional resistance to sliding by invoking support from the passive pressures from the core of the breakwater.

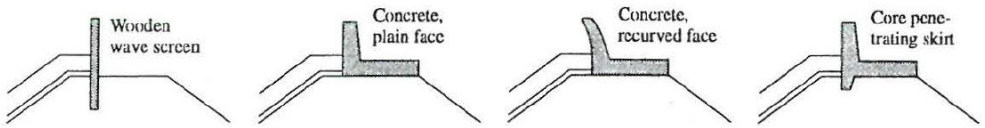

Figure 6: Different crown wall lay-outs (Pedersen, 1996).

The different advantages of building a rubble mound breakwater with a crown wall and their relative necessity for a given project are important for the design of the crown wall. A typical procedure for the calculation of crown wall dimension is described by Martin: " *i) The rate of wave overtopping determines the crest level of the crown wall. ii) The construction procedure and costs governs the crown wall foundation level. And finally, iii) a stability analysis determines the width and the other dimensions of the crown wall*" (Martin et al., 1999). A detailed description and analysis of the different methods that are used to design a crown wall are given in section 3.

Governing parameters

In this description Martin already mentions some key parameters and dimensions that characterise a crown wall. Figure 7 show these parameters and more.

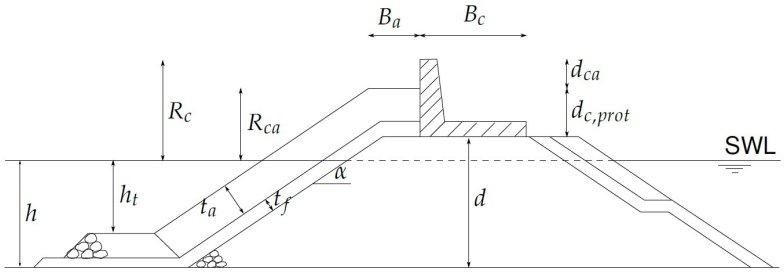

Figure 7: Typical rubble mound breakwater with crown wall cross section (CIRIA, 2007).

From left to right we distinguish:

- Water depth - h
- Depth of toe below SWL - h_t
- Crest freeboard - R_c
- Armour crest freeboard - R_{ca}
- Armour thickness - t_a
- Filter thickness - t_f
- Slope angle - α
- Armour berm width - B_a *(- Typically also indicated as crest berm width -* G_c *)*
- Structure width - B_c
- Structure height - d
- Unprotected crown wall height - d_{ca}
- and protected crown wall height - $d_{c,prot}$
- *not yet in the figure: foundation level -* F_c*, defined by h-d here.*

Wave loading and failure

The wave load on the structure is heavily influenced by the breaking process of the wave onto the structure. There are several types of wave breaking, typically differentiated by the surf similarity parameter: $\xi_m = tan\alpha / \sqrt{\frac{H_s}{L_{m0}}}$. The most relevant types of breaking for this study are shown in figure 8, as suggested by Battjes (1974).

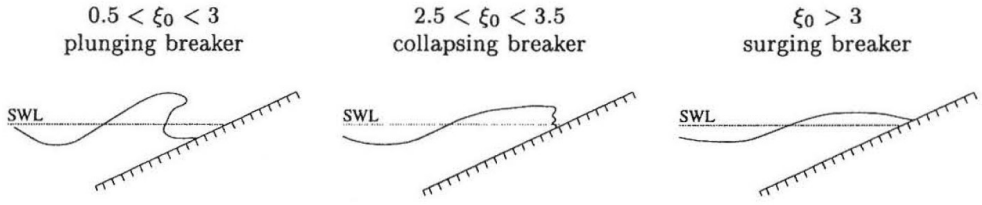

Figure 8: Relevant wave breaking types (Pedersen, 1996).

The run-up of the wave over the armour layer to the crown wall is the first important and most obvious impact. This causes a horizontal force on the wall face as well as inducing an overturning moment. As the wave penetrates the core of the breakwater, the pore water pressure might increase on the underside of the crown wall introducing an uplift force and an accompanying overturning moment.

A simple free-body diagram is shown in figure 9. It illustrates the horizontal and vertical forces with the corresponding moments as well as showing an indication of what the pressure distribution over the wall faces might look like and. The grey and black arrows refer to forces by the armour layer on to the crown wall and the self-weight respectively. Deviations from this indication in design methods are detailed in section 3.

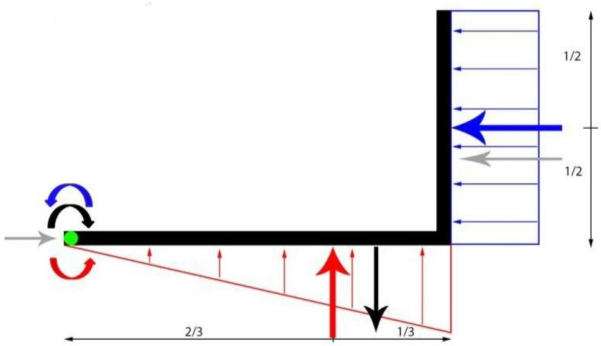

Figure 9: Free body diagram showing the forces, pressures and moments working on a crown wall (Van Heemst, 2014).

These loads threaten the stability of the crown wall which is crucial for the overall safety of the breakwater. A failure of the crown wall might lead to a total breakdown of the whole structure, as more vulnerable parts are exposed to wave loads and large parts of the breakwater are washed away. Different magnitudes and combinations of the horizontal and vertical loads can lead to the failure modes that are shown in figure 10, the first of which is arguably the most common one. Sliding occurs when the frictional resistance is exceeded by the horizontal load. In the case of a penetrating skirt (shown in figure 6), not only friction but also passive soil pressure resists the sliding. *Overturning* is the failure due to a critical overturning moment, which is typically a combination of a horizontal force on the wall face and a uplift on the wall base. Overturning is often difficult to identify since only small rocking movements of the crown wall could be visible. This rocking decreases the contact surface of the crown with the breakwater, which could lead to sliding (Pedersen, 1996). The final two failure modes are not covered in the stability analysis of the study, but are briefly mentioned here for completeness. *Cracking* is a failure of the structural strength of the wall. Not only the wave loading plays a role here but also the long term strength decreases of the wall during its lifetime. *Geotechnical* failure is a failure of the breakwater itself under the wave loads and the weight of the crown wall.

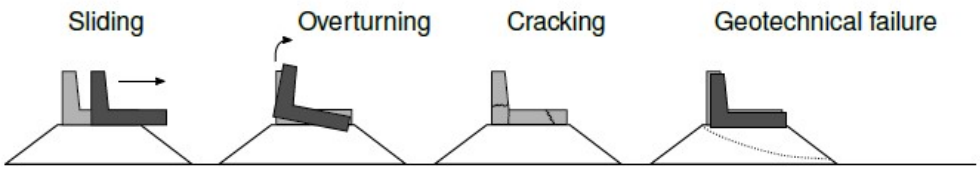

Figure 10: Crown wall failure modes (Pedersen, 1996).

Stability criteria

Using the simplified depiction of wave loads (figure 9) stability criteria for sliding and overturning can be formulated. In sliding the main resistance comes from the self weight of the crown wall which ensures friction between it and the layer on which it rests. The loading is a combination of a horizontal force and the reduced vertical loading due to uplift pressures on the crown wall. The criterion is the following:

$$\mu_s(F_g - F_{v,max}) \leq F_{h,max} \text{ or} \tag{2a}$$

$$\text{Factor of Safety} = \frac{\mu_s(F_g - F_{v,max})}{F_{h,max}} \tag{2b}$$

here μ is the friction coefficient, which ranges from 0 to 1, F_g is the product of the gravity based mass (reduced by the weight of the submerged volume of the crown wall) and the gravitational acceleration g.
For the overturning failure mode similarly we can formulate the criterion:

$$M_g - M_v \leq M_h. \tag{3}$$

Here the moments are shown as curved arrows and calculated about the heel of the crown wall as shown in figure 9.

3 Literature Review

In this chapter the existing methods for calculating wave forces on crown walls are covered. Apart from a description of the method also a critical analysis of it is provided, to help formulate the knowledge gap in the field of crown wall designs. Most of these methods are based on small-scale model tests in wave flumes. The results from these tests then allow for an empirical formulation of wave forces. The different methods are covered more or less in chronological order starting with the method formulated by Günback and Göcke.

The authors that are covered in this section build on earlier works, a few of which are briefly mentioned here. Decades ago Jensen (1984) already formulated a relation between horizontal wave force and wave height and length, armour crest freeboard and crown height, as well as analysing the effect of oblique waves. These findings were in part confirmed by Bradbury (1988), who tested on several different rock slope configurations. A few years later, Hamilton & Hall (1993) formulated a different approach by relating the aforementioned parameters to the minimal stable mass of a concrete crown wall for stability, as well as investigating the effect of a penetrating skirt (see 2.2). For all their configurations with a skirt the failure mode was overturning, whereas all non-skirt walls failed by sliding.

3.1 Existing design methods - Crown walls

Günback and Göcke

(Note to commission: I was not able to obtain the original paper, so all my descriptions and conclusions are based on second-hand sources)
Based on the results of their small-scale physical model test, Günback and Göcke described the wave loading as a function of a virtual run-up. This virtual run-up is a proxy for the wave energy that needs to be dissipated by the crown wall. This is separated into two parts. Firstly, the hydrostatic pressure that would have been created if the slope was infinitely long. Secondly, an impact pressure is formulated. These two are summed and assumed to happen simultaneously, to calculate the total pressure. The vertical load on the wall is taken to be a linear pressure distribution, starting from a hydrostatic assumption at the toe and zero at the rear of the crown wall base.

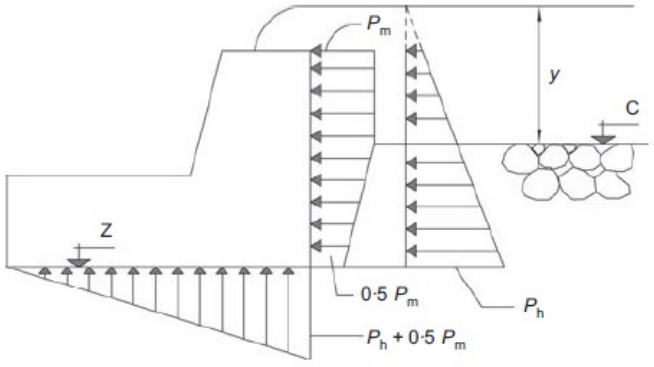

Figure 11: Indication of parameters and assumptions of method by Günback and Göcke (Pedersen, 1996).

Method
The impact pressure (P_m) is described as follows

$$P_m = \frac{\gamma_w(\sqrt{g \cdot y})^2}{2g} = \frac{\gamma_w}{2} y,$$

which is reduced to half its full value for the sheltered part of the wall face. The hydrostatic pressure is quite simple, with the definition of the length over which it works and the run-up as follows:

$$P_h = \gamma_w y$$

$$y = \frac{R_U - A_c}{sin\alpha} \frac{sin\theta}{cos(\alpha - \theta)}$$

$$R_U = \begin{cases} 0.4H, & \text{if } \xi_m < 2.5. \\ H, & \text{if } \xi_m > 2.5. \end{cases} \tag{4}$$

Discussion

As one of the earliest methods of estimating wave forces it can be expected that significant criticism can be given to the Günback and Göcke method. Firstly, regular waves were used in the physical model tests. This can give an indication but is not representative of typical wave conditions found on actual sites. Secondly, the reduction factor given to the impact pressure of the sheltered wall face is taken to be 0.5. This is taken to be a constant factor independent of breakwater geometry, whereas critical inspection would suggest that at the very least armour crest width should influence this reduction (this and more was later confirmed by Martin et al. (1999)). Other important criticisms include lack of clarity of definitions in the paper. The wave height that is expected to be used in the method is not specified. The range of applicability is not mentioned either, just that can be used for 'wave screen' type structures. This is especially important since only a limited amount of geometries are tested in the model tests.

Martin

Concluding that previous methods where inadequate (Iribarren and Nogales (1964) too conservative, Jensen (1984) not including wave period and Günback and Göcke (1984) is too difficult to apply (Martin et al., 1999)), Martin formulated a new semi-empirical method for describing forces on crown walls. Martin used data from 51 model test on breakwaters with varying armour crest berm width and armour size using mostly regular waves. With the waves breaking on the armour, Martin mentions that his method is only valid for waves rushing up to the crown wall, not for when they break on it.

Method

An overview of the parameters that Martin describes and uses can be found in figure 12.

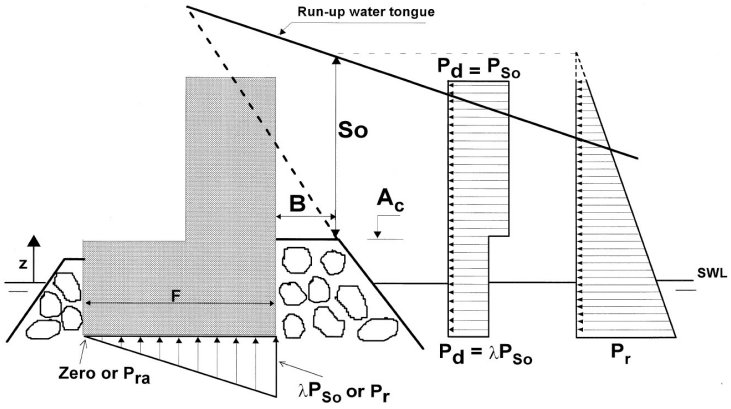

Figure 12: Indication of parameters and assumptions of method by Martin (Martin et al., 1999).

Similarly to Günback and Göcke, Martin differentiates between two pressures: one for the abrupt change of direction of the bore (*dynamic pressure*), which has a value for both the sheltered and unsheltered part of the wall and one for maximum run-up, due to down-rushing of the water mass (*reflecting pressure*). This is linear along the full length of the crown wall. Contrary to Gunback and Gocke, Martin distinguishes two load situations, namely the maximum horizontal dynamic and the maximum horizontal reflecting pressure. The stability of the crown wall is judged in both situations.

The impact or dynamic pressure of the wave on the unprotected part of the crown wall is found using

$$p_i(z) = p_{so} = c_{wl}\rho_w g S_0,$$

where

$$S_0 = H\left(1 - \frac{R_{ca}}{R_u}\right)$$

and

$$c_{wl} = 2.9\left(\frac{R_u}{H}cos\alpha\right)^{-2}.$$

For the *protected* part of the crown wall an empirical reduction factor is introduced which is a function of the wavelength and armour crest width, namely

$$c_{w2} = 0.8e^{-10.9B_a/L}.$$

To formulate the run-up that helps determine the horizontal impact, Martin uses the equation for run-up on regular waves as proposed by Losada & Gimnez-Curto (1980):

$$\frac{R_u}{H} = Au\big(1 - e^{B_u \cdot \zeta_m}\big),$$

in which Au and Bu are dependent on the armour type on the slope. The reflecting pressure is found using a hydrostatic formulation, namely

$$p_p = c_{w3}\rho_w g(S_0 + R_{ca} - z),$$

with

$$c_{w3} = a \cdot e^{c(\frac{H}{L} - b)^2}.$$

Here a, b and c are non-dimensional coefficients and c_{w3} is a reduction factor for the number of armour units in front of the crown wall (a measure for the armour crest width).

Lastly, the uplift pressure is linear, but not automatically taken to be zero at the rear end, as in other methods. Martin formulates two values, the maximum value at the toe (p_{re}) and the minimum value at the rear (p_{ra}), as follows:

$$p_{re} = p_p$$

and

$$P_{ra} = \frac{B_c}{L_p} p_{re}.$$

Discussion

Martin is considered to be a considerably more robust method than previous ones, mostly because of its separation of two types of loading and the inclusion of many (relevant) parameters (Negro Valdecantos et al., 2013). Specifically the separation between the dynamic wave pressure and the (qausi-) hydrostatic one is an important one since it describes the actual physical process quite well. The addition of extra parameters that take into account the geometry of the breakwater, also speak for this method. This includes the width of the armour crest berm.
An important criticism though is that in the test regular waves are used, which is not a representative wave condition for actual designs. It is worth saying that Martin does formulate a method to expand these measurements to work for irregular wave conditions. Another criticism is that the method has been validated using a breakwater which is not really representative since it has a fairly peculiar cross section (Negro Valdecantos et al., 2013). Moreover, similarly to Günback and Göcke, Martin does not specify which wavelength is used in his method. The reader is left to guess whether it is H_s, $H_{0.1\%}$ or something else. Negro Valdecantos et al. (2013), also points out that the Au and Bu parameters used to calculate the run-up are incoherent, since less run-up is indicated for cube-type elements when compared to rock. The opposite should be expected with the lower roughness of smooth cubes.

Pedersen

Using the results from his 373 test with approximately 5000 waves each, Pedersen described an extensive formulation for the wave horizontal and vertical wave forces on crown walls under wave loads. In the test several breakwater cross sections were investigated, with different types of armour (rock armour - cubes - Dolos), varying crown hall height, crest berm width and the slope. The wave climate was characterised by both surging and collapsing deep water waves (h/L$>$ 4). Pedersen concluded that wave forces are dominated by wave impact, which translates to the stagnation of water that is running-up the slope. This forcing is reduced for the protected part of the wall face. Vertical forces were not measured but assumed to be linear under the crown wall base, approximated by the hydrostatic assumption at the toe of the wall and taken to be zero at the end of the underside (figure 13).
Pedersens method has been quite important in recent decades and has been implemented in the US Army Corps of Engineers (2002) as a leading design method.
Method

Firstly, Pedersen formulates the horizontal impact pressure of the unprotected part of the wall as follows:

$$p_m = g\rho_w(R_{u,0.1\%} - R_{ca}),$$

in which R_u is the run up height, which is exceeded by 0.1% of the waves, as formulated by Van der Meer & Stam (1992):

$$\frac{R_{u,0.1\%}}{H_s} = \begin{cases} 1.12\zeta_m, & \text{if } \zeta_m \leq 1.5. \\ 1.34\zeta_m^{0.55}, & \text{if } \zeta_m > 1.5. \end{cases} \tag{5}$$

where ζ_m is the Iribarren parameter as described in section 2.2. This p_m is shown in the figure below. It also shows that Pedersen assumes a reduction factor of 0.5 for the sheltered part of the vertical wall face.

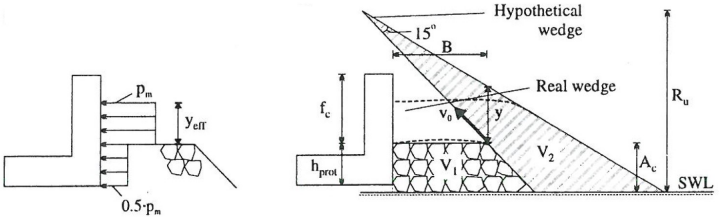

Figure 13: Indication of parameters and assumptions of method by Pedersen (Pedersen, 1996).

Similar to the method of Günback and Göcke, Pedersen formulates a hypothetical and real run-up wedge which can be seen in figure 13. They are a measure for the incoming wave energy. The hypothetical wedge run-up has a thickness of

$$y = \frac{R_{u,0.1\%} - R_{ca}}{sin(\alpha)} \cdot \frac{sin(15°)}{cos(\alpha - 15°)}.$$

The real wedge quantifies the run-up that is relevant for the structure and has a thickness y_{eff}, which can be found using

$$y_{eff} = min\{\frac{y}{2}, d_{ca}\}.$$

The 1:1000 total horizontal force is then ultimately found using

$$F_{H,0.1\%} = 0.21\sqrt{\frac{L_{0m}}{B_a}}(1.6p_m y_{eff} + V\frac{p_m d_{c,prot}}{2}).$$

Pedersen urges to only use the equations in the parameter range of the test and thus the range in which the formulation was validated. These ranges are given in table 2.

Parameter	Range
ξ_m	1.1-4.2
H_s/A_c	0.5-1.5
R_c/A_c	1-2.6
A_c/B	0.3-1.1
$\cot\alpha$	1.5-3.5

Table 2: Applicability range of Pedersens method (Pedersen, 1996).

Discussion

Pedersens paper has been widely regarded as a really important step in describing the wave loading on crown walls. This study includes a large amount of tests and many waves per test, so there is

a large data set to work with. Also many different (potentially) influential parameters are varied and tested. Crucially, Pedersen is quite precise in his formulation and the different parameters are well defined. The range of application is also clearly indicated, ensuring that applying his method can be done with some confidence.
An important criticism of Pedersen is that in his research he does not look at uplift pressures at all. It is only briefly stated that measuring these pressures is impossible due to strong scaling effects and that typically a triangular distribution is used if the foundation is above MSL. The actual formulation is not found in his method. Pedersen does mention that his approach of uplift yields conservative estimates. In the calculation of the overturning moment, the contribution of uplift is not taken into account, which could be considered an underestimation.

Nørgaard

Some 17 years after the publication of the state-of-the-art method by Pederson, Nørgaard - a researcher from the same group as Pedersen - proposed an extension to the method outlined in the previous section. His main criticism is that its formulas '*are not validated for depth limited design conditions which are present at many sites*' (Nørgaard et al., 2013). To extend the method to these depth limited conditions Nørgaard performed 162 small scale tests in both deep and shallow water using different geometries (varying the protected fraction of the crown wall) and with improved sensors. This way Nørgaard could improve and extend the applicability of Pedersens method.

Method

Firstly, Nørgaard suggests adapting the use of H_s by Pedersen to $H_{0.1\%}$ in equation (5). Leading to the following modified equations:

$$R_{u,0.1\%} = \begin{cases} 0.603 \cdot H_{0.1\%}\zeta_m, & \text{if } \zeta_m \leq 1.5. \\ 0.722 \cdot H_{0.1\%}\zeta_m^{0.55}, & \text{if } \zeta_m > 1.5. \end{cases} \tag{6}$$

Comparing his with the results from Pedersen, Nørgaard concludes that Pedersens sensors misidentified the horizontal forces somewhat, as these sensors are influenced by dynamic amplification. To account for this a small adaptation is made for the empirical factor (b changed from 1.6 to 1) used in the calculation of the horizontal force estimation:

$$F_{H,0.1\%} = 0.21\sqrt{\frac{L_{0m}}{B_a}}(p_m y_{eff} + V\frac{p_m d_{c,prot}}{2}).$$

The last adaptation is made in the formulation of the overturning moment. Nørgaard introduces two coefficients that take into account the point of attack of the load as the protected fraction of the wall face varies.

$$M_{H,0.1\%} = (h_{prot} = 0.5 \cdot y_{eff} \cdot e_2)F_{Hu,0.1\%} = 0.5h_{prot}F_{Hl,0.1\%} \cdot e_1,$$

where

$$F_{Hu,0.1\%} = 0.21\sqrt{\frac{L_{m0}}{B}}p_m \cdot y_{eff},$$

$$F_{Hl,0.1\%} = 0.5 \cdot 0.21\sqrt{\frac{L_{m0}}{B}}p_m \cdot V \cdot d_{c,prot},$$

$$e_1 = 0.95 \text{ and } e_2 = 0.40$$

An important reason for this study was the extension to depth limited conditions. This new and extended range of application can be found in table 3. A distinction is made between fully protected ($d_{ca} = 0$) and partly unprotected ($d_{ca} > 0$) wall faces.

Parameter	Range $d_{ca} = 0$	Range $d_{ca} > 0$
ξ_m	2.3-4.9	3.31-4.64
H_s/R_{ca}	0.5-1.63	0.52-1.14
R_c/R_{ca}	0.78-1	1-1.7
H_{m0}/h	0.19-0.55	0.19-0.55
H_{m0}/L_{m0}	0.018-0.073	0.02-0.041

Table 3: Applicability range Nørgaards method (Nørgaard et al., 2013)

Discussion

The adaptation by Nørgaard can be seen as a good an important one. An already quite solid method is reformulated somewhat to incorporate more data and, crucially, a wider set of parameters, enabling the use of the method in depth-limited conditions.
The uplift concerns of Pedersens method are not directly tackled though. No adaptations are suggested for the calculation of the vertical pressure distribution on the crown wall base. Nørgaard, however, is not oblivious to this fact he did measure the vertical pressures. He does not formulate an improved method, but does in fact mention that the maximum uplift pressures and the maximum horizontal pressures do not seem to occur simultaneously. Not taking this into account should clearly yield more conservative estimates. This is acknowledged by Nørgaard. Lastly, it is mentioned that the proposed method will not give good estimates for long waves. In swell-wave climates, then, this method could not be used to predict wave loads.

Bekker

Following the work of Nørgaard, Bekker did additional small-scale model tests and compared his results with both Pedersens and Nørgaards methods. Most attention was focussed on improving understanding and often overconservative uplift pressure and the time lag between what Martin refers to as the dynamic and reflecting impact. Also, critical weights as a measure for stability are introduced similarly to Hamilton & Hall (1993).

Method

To determine Bekkers dimensionless critical mass (or minimal stable mass) four equations are formulated, differentiated by the wave steepness (swell - $s_{op} = 0.01$ & storm $s_{op} = 0.04$) and whether H_s or $H_{0.1\%}$ is used. This can be summarised as:

$$W^*_{crit,swell} = \begin{cases} 0.83\dfrac{H_s^2}{R_{ca}^2} + 0.03, & \text{if } 0.50 \leq H_s^2/R_{ca}^2 \leq 2.20. \\ 0.25\dfrac{H_{0.1\%}^2}{R_{ca}^2} + 0.18, & \text{if } 1.00 \leq H_{0.1\%}^2/R_{ca}^2 \leq 6.60. \end{cases} \tag{7}$$

$$W^*_{crit,storm} = \begin{cases} 0.62\dfrac{H_s^2}{R_{ca}^2} - 0.23, & \text{if } 0.50 \leq H_s^2/R_{ca}^2 \leq 2.20. \\ 0.21\dfrac{H_{0.1\%}^2}{R_{ca}^2} - 0.19, & \text{if } 1.00 \leq H_{0.1\%}^2/R_{ca}^2 \leq 6.60. \end{cases} \tag{8}$$

The dimensionless critical mass is defined as:

$$W^*_{crit} = \frac{W_{crit}}{\mu_s \rho_w g B_c d_c}.$$

Additionally, Bekker proposes a reduction factor to supplement Nørgaards method for estimating the uplift pressure. This reduction factor takes into account the reduced length over which the uplift pressure works and is defined as $\gamma_v = x_c/B_c$ (a visual representation of x_c can be found in figure 3). The reduction factor that can be applied is similarly found now using six equations, namely

$$\gamma_{v,swell} = \begin{cases} 0, & \text{if } H_s/R_{ca} \leq 0.64. \\ 2.41\dfrac{H_s}{R_{ca}} - 1.54, & \text{if } 0.64 \leq H_s/R_{ca} \leq 1.05. \\ 1, & \text{if } H_s/R_{ca} > 1.05. \end{cases} \tag{9}$$

$$\gamma_{v,storm} = \begin{cases} 0, & \text{if } H_s/R_{ca} \leq 0.75. \\ 2.41\dfrac{H_s}{R_{ca}} - 1.54, & \text{if } 0.75 \leq H_s/R_{ca} \leq 1.34. \\ 1, & \text{if } H_s/R_{ca} > 1.34. \end{cases} \tag{10}$$

The application range for these formulas can be found in the table below.

Parameter	Range
H_s/R_{ca}	0.71-1.48
H_s/L_{0p}	0.01; 0.04
B_a/d_a	1.88
d_c/d_a	1.88
$d_{50,c}/d_{50,a}$	0.40
$(d_{85}/d_{15})_c$	1.39
$(d_{85}/d_{15})_a$	1.45
$\cot\alpha$	2

Table 4: Applicability range of Bekkers reduction factor and critical weights (Bekker et al., 2018).

Discussion

The method as proposed by Bekker seems quite promising. The idea to refine the contact surface between the excess water pressures and the underside of the crown wall seems to work quite well. Both his own test and the reformulation of Pedersen and Nørgaards methods seem to estimate wave forces quite well.

Important criticisms of his work include the fact that this reduction factor was mainly determined by visual inspection of the contact surface of the water and the underside. Bekker mentions that the colour of the set-up and the camera resolutions were bottlenecks in determining this value correctly. Moreover, Bekker quite extensively covers the issues that were encountered with data collection and analysis, since the pressure sensors were quite prone to record a noisy signal. To counter this heavy filtering of the data was done. This could and would have greatly altered the conclusions that were drawn from the data set.

Molines

Most methods that have been mentioned are quite similar in their approach to finding a good estimator of wave forces on crown walls. Molines et al. (2018) proposed a quite different approach

to tackle this problem. He describes his decision to do so as follows: "*From the conceptual point of view, this study changes the virtual wave run-up for the wave overtopping as the key variable to estimate wave forces and overturning moments on the crown wall. It is not possible to measure virtual run-up and, compared to wave forces on crown walls, overtopping discharge can be measured easily in small-scale tests and prototypes. Therefore, the overtopping rate is a reasonable explanatory variable to estimate forces on the crown wall.*" Overtopping also implicitly takes into account parameters like permeability of the filter and the core. In order to formulate his new method, Molines uses the data from 250 tests from Pedersen (1996) and Smolka et al. (2009) and using a neural network attempt to formulate a whole range of better estimators of wave forces on crown walls, most notably using overtopping.

Method

For the horizontal wave force Molines introduces a very simple formula and a more complex and better estimating one, namely

$$\frac{Fh_{0.1\%}}{0.5\rho g C_h^2} = 3.6 + 0.6 logQ$$

and

$$\frac{Fh_{0.1\%}}{0.5\rho g C_h^2} = (0.23 + (logQ + 6)(0.27 ln(\zeta_{0p}) + 0.1)\big(0.5\frac{R_c - A_c}{C_h} + 1\big) - 0.15.$$

For the uplift pressure two distinct cases are identified. The first one is the uplift pressure measured for 0.1% of the waves (Pb) and the second one is the uplift pressure that is measured simultaneously with the max horizontal wave force measured for 0.1% of the waves (PbF). For the maximum uplift pressure Molines also formulated two equations (a simple and a better estimating one), this was nts, however, done for the PbF:

$$\frac{Pb_{0.1\%}}{0.5\rho g C_h} = 4.3 + 0.52 logQ,$$

$$\frac{Pb_{0.1\%}}{0.5\rho g C_h} = 0.9 + \big(0.4\frac{R_c - A_c}{C_h} + 0.6\big)(logQ + 6)$$

and

$$\frac{PbF_{0.1\%}}{0.5\rho g C_h} = 0.02\big(\frac{F_c}{L_{0p}}\big)^{-1/2}.$$

For the overturning moments the same distinct cases are identified. Two (simple and better estimating) due to the horizontal forces exceeded by 0.1% of waves (Mh) and one due to horizontal forces simultaneous with $Fh_{0.1\%}$ (MhF).

$$\frac{Mh_{0.1\%}}{\rho g C_h^3} = 0.7 + 0.11 logQ,$$

$$\frac{Mh_{0.1\%}}{\rho g C_h^3} = 0.15 + \big(0.3\frac{R_c - A_c}{C_h} + 0.09\big)(logQ + 5)$$

and

$$\frac{MhF_{0.1\%}}{\rho g C_h^3} = 1.08 + 0.18 logQ.$$

The method is suggested to only be used in the parameter range as indicated in table 5.

Parameter	Range
$R_c/(\gamma_f H_{m0})$	1.67-6.55
ξ_m	1.39-7.77
$\gamma_f R_{u0.1\%}/R_c$	0.36-1.41
$(R_c - A_c)/C_h$	0.00-0.59
F_c/L_{0p}	0.00-0.03
logQ	-6.00 - (-2.78)

Table 5: Applicability range of Molines' method (Molines et al., 2018).

Discussion

Molines has done quite a lot of work over the last five years to introduce, test and ensure that his new method estimates wave forces well. In the paper Molines & Medina (2016), first reformulate a new wave overtopping estimator that will later lay the foundation for its wave force estimators. Ambitiously, it compares its own estimator with the CLASH project (as described by Verhaeghe et al. (2004) and Steendam et al. (2005)), that was rigorously tested by M. R. van Gent et al. (2007). This new estimator seems to be working quite well, but the paper's more important goal seems to be to describe the physics of the overtopping phenomenon more intuitively by formulating a simple (or simpler) expression. Its criticism of the neural network expression is that it is a black-box. The black-box criticism is not the strongest one as the neural network was carefully set-up and a relation between what goes in and goes out could definitely be formulated.

The paper mentions repeatedly that wave overtopping measurements are easy and precise. This is an important reason why the use of this parameter is proposed for this method. This favourable description of overtopping could be questions as the need for a huge data set to formulate a neural network based overtopping estimator (CLASH project), could be seen as an indication that wave overtopping is indeed quite complex and difficult to predict. Were the argument of cheaper measuring, compared to pressure, seems quite valid, the precision and ease of measuring overtopping is questioned.

Importantly, the proposed method does not estimate horizontal wave forces and turning moments on crown walls better that existing alternatives. Franco et al. (2018), however, does conclude with its model tests that indeed *"mean overtopping discharges are correlated with the dimensionless horizontal force induced on the wall as proposed by Molines et al. (2018)"*. These estimations are not compared to other methods. These conclusions ignore the reality that mean overtopping rates are averages over a time span whereas for forces the focus is on extremes.

Lastly, somewhat remarkably Molines et al. (2018) insists that its formulations are much simpler than other contemporary methods for estimating wave forces. This could be argued after a quick glance through the discussed design methods in this sections. This, however, glosses over the obvious fact that its formulation include the variable Q and that - if no overtopping discharge data is available - it should be estimated using the formulations from CLASH or Molines & Medina (2016), which are decidedly complex formulations.

For uplift, Molines' predictions do work quite well, which is promising. However, only some of these formulations include overtopping as a contributing parameter.

Concluding, the method as introduced by Molines seems to work relatively well in estimating wave forces on crown walls. The separation from the actual driving physical process of wave loading (by using overtopping, instead of measured pressures) is intuitively not very satisfactory. It does, however, seem to give reasonable first estimates that could be used as first design benchmarks.

3.2 Conclusions

The description of the load characteristics of rubble mound breakwater crown walls is a complex area of study that has received significant attention through model test studies. While early studies focused on horizontal forces, current estimators have produced good results for these loads, but have missed the mark for longer waves. In contrast, vertical forces have been sparsely studied, and proposed methods for estimating these forces seem to overestimate their impact or magnitude, particularly the influence of the foundation level, which remains poorly understood. Additionally, other parameters such as the armour crest width and porosity have not been rigorously tested for their influence on the loading. The time lag between maximum horizontal and maximum vertical force is an important phenomenon that has been mentioned in multiple papers but lacks a physical explanation, with only Martin et al. (1999) providing a design rule that considers it. Finally, overtopping has been proposed as a force estimator, but it is not considered in this study because it seems incoherent to use a mean parameter to estimate extreme forces and because a lower crown wall would actually result in larger overtopping and smaller forces, contradicting this proposal.

4 Physical Model Set-up

This chapter outlines the details of the physical model that is used to fulfil the objectives and answer the research questions described in section 1.3. The reference prototype and the scaling laws are described along with a detailed description of the scale model, instrumentation and experiments.

4.1 Scaling

Modelling large structures in smaller scales is an established method of study in the field of hydraulic engineering. This ensures more controlled conditions (in a lab) at a fraction of the cost and time investment of a large scale model. Most conclusions drawn that are accepted in the literature come from this sort of experiments (see section 3). With its clear benefits come drawbacks. Differences between model and prototype may lead to model, scale and measurement effects. *Model effects* arise with discrepancies between the model and prototype, like in the geometry of the structure or the wave conditions that the model is subject to. Inconsistencies in the measurement techniques between the model and the prototype are classified as *measurement effects*. Finally, *scale effects* are discrepancy in relevant force ratios. These effects typically increase with the scale factor defined as the ratio between a characteristic length scale in the prototype (L_p) and the model (L_M) (Heller, 2011):

$$\lambda = \frac{L_p}{L_M}. \tag{11}$$

Model effects are not of primary concern for this study, as there is not a specific prototype on which the scale model is based, because this is not a typical stability test for an existing breakwater design. Instead, the breakwater designed by Van Oord for the port in Map Ta Phut, Thailand is used as a reference. This somewhat typical breakwater geometry,with a relatively simple cross section can be found in figure 14. It shows a double layer of rock armour on a quarry run core, with a simple toe configuration. The crown wall sits directly atop the core material, has a partially protected and unprotected vertical face and its base is located about 20 centimetres above DHWL.

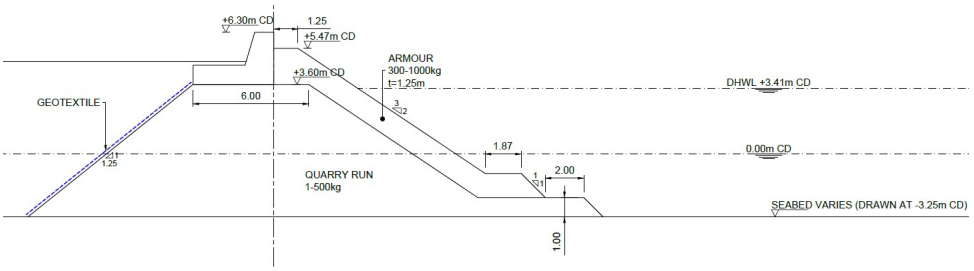

Figure 14: Final design of Map Ta Phut breakwater as proposed by Van Oord.

In contrast to model effects, scale effects are of concern for this study and thus the concept will be elaborated on in detail in the next section.

Scale effects and similarities

A model with no scale effects, that is completely similar to its prototype is referred to as *mechanically similar*. This implies three types of similarity, namely geometric, kinematic and dynamic. *Geometric similarity* is the simplest form which only involves similarity in shape (like a model car), model lengths then scale with λ and areas and volumes scale with λ^2 and λ^3, respectively. *Kinematic similarity* implies similarity of motion along with geometric similarity, so not only length scales but also time scales are modelled correctly (and thus velocities, accelerations, discharges etc).

Finally, *dynamic similarity* also implies that force ratios are similar along with the constraints of geometric and kinematic similarity. Scaling laws that ensure dynamic similarity and thus constant force ratios are used to calculate the different parameters that are used in the model. These laws relate a specific force to the most relevant force in fluid dynamics, namely the inertia force. A few important ones relate inertia to the gravitational force (Froude), viscous force (Reynolds) and surface tension force (Weber)

A model that is completely similar to its prototype with no scale effects is called "mechanically similar." This implies geometric, kinematic, and dynamic similarity. Geometric similarity involves similarity in shape, where model lengths scale with λ, and areas and volumes scale with λ^2 and λ^3, respectively. Kinematic similarity adds similarity of motion, including time scales. Dynamic similarity adds similarity of force ratios, which are calculated using scaling laws that relate specific forces to the inertia force (Heller, 2011). Froude, Reynolds, and Weber are important scaling laws that relate inertial to gravitational, viscous, and surface tension forces, which are defined as:

$$\text{Froude number} = Fr = \left(\frac{inertial\ force}{gravity\ force}\right)^{1/2} = \frac{u}{\sqrt{gL}},$$

$$\text{Reynolds number} = Re = \frac{inertial\ force}{viscous\ force} = \frac{uL}{\nu} \text{ and}$$

$$\text{Weber number} = We = \frac{inertial\ force}{surface\ tension\ force} = \frac{\rho u^2 L}{\sigma},$$

where

u	[m/s]	= flow velocity
L	[m]	= characteristic length
g	$[m/s^2]$	= gravitational acceleration
ν	$[m^2/s]$	= kinematic viscosity
ρ	$[kg/m^3]$	= density of water
σ	$[kg^2]$	= surface tension

Resolving for multiple dimensionless numbers simultaneously is very complex in practice. Resolving both Reynolds and Froude similarity for example requires a significant adaptation of the kinematic viscosity of the fluid that is used in the model, as compared to the water that interacts with the prototype. It's thus typically impossible to find an apt fluid for most scales, which inhibits true similarity (Frostick et al., 2011). How the scaling is done and the relative importance of different forces in this study is described next.

Geometric similarity

The main restrictions in the design of the cross section of the model and hydraulic boundary conditions are the ones set by the flume. For the wave flume in the WaterLab (see section 4.2) a maximum of 0.60m water level in combination with a 0.15m significant wave height is used as a general rule of thumb. Opting for a core crest height of 0.60m ensures that the structure is as large as possible while allowing for a limiting case where waterline is at same level as the crown wall base, as in the experiments of Martin et al. (1999) and Pedersen (1996) (note: this water level is not chosen for the base case in this study). This choice sets the length scale to about 1:12 (see figure 14). Since the experimental set-up is not strictly modelled after the prototype, the scale ratio is somewhat hypothetical and merely serves as an indication.

Froude similarity

Since gravitational forces are dominant in the flume with the envisioned set-up, Froude scaling is the main scaling that is taken into account. To do this the definition of the Froude number is used to find the scaling of the most important variables in this study, namely wave heights, periods, masses, forces, pressures and discharges. The scale factors of these individual parameters are set by the restriction that the Froude scale factor is 1, which is derived from the original assumption that the Froude number is the same in the model and the prototype as follows:

$$\left(\frac{u}{\sqrt{gL}}\right)_{prototype} = \left(\frac{u}{\sqrt{gL}}\right)_{model},$$

$$\frac{u_p}{u_m} = \sqrt{\frac{g_p L_p}{g_m L_m}},$$

$$n_{Fr} = 1 = \frac{n_u}{\sqrt{n_g n_L}}.$$

Here n_L is equal to λ in equation (11) and n_u and n_g are defined similarly to λ. Using this and defining in terms of n_L the scaling relations to the other parameters are found, namely:

$$\begin{array}{lcll} n_T & = & n_L^{0.5} & \text{- Time (s)} \\ n_u & = & n_L^{0.5} & \text{- Velocity (m/s)} \\ n_M & = & n_\rho \cdot n_L^3 & \text{- Mass (kg)} \\ n_F & = & n_\rho \cdot n_L^3 & \text{- Force (N)} \\ n_p & = & n_\rho \cdot n_L & \text{- Pressure (N/m}^2\text{)} \end{array}$$

Reynolds similarity

As elaborated in the previous section, both Reynolds and Froude similarity cannot practically be achieved simultaneously. Fortunately, scale effects from viscous forces taken into account by Reynolds number are small when friction plays an small role, this is the case for waves travelling relatively short distances. Also, large ranges of the Reynolds number have a constant drag coefficient. So - as is the case for this study - for waves in a flume, where the Reynolds scale is in the same range for the model and the prototype the Reynolds number need not be exactly the same in the model and prototype (Wolters et al., 2010).

Weber similarity

In most prototype scale scenarios the surface tension force is insignificant to the inertial one. So, to comply with Weber similarity this should also be the case for the model. In this scenario similarity is not directly fulfilled because $n_{We} = 1$, but rather because We_{model} and $We_{prototype} << 1$. To ensure this is the case typically wave lengths have to be larger than 3cm (5cm design wave) and wave periods should be larger than 0.35s (Frostick et al., 2011), (Wolters et al., 2010). If these conditions are not met wave motion damping will alter the conditions as compared to the prototype.

Permeability similarity

As expanded on before, Reynolds scaling is not strictly necessary for short travelling waves and certain ranges of the Reynolds number. However, in small scale models viscous forces might be significant for the wave-driven flow inside the core or filter of a breakwater. This is due to the smaller rocks, which allow for smaller pores, through which the flow has a more significant viscous

component. These scale effects are often mitigated by scaling based on permeability and correcting the diameter of the rocks. This is usually achieved through similarity of hydraulic gradient by using the Forchheimer equation (Frostick et al., 2011):

$$I_m = I_p = au_f + bu_f|u_f|,$$

where I is the hydraulic gradient, u_f is the depth-averaged filter velocity, and a and b are friction coefficients representing the relative importance of the Darcy or turbulent flows based on M. van Gent (1995a) and M. van Gent (1995b). If, however, the rock diameter - in the model as found through Froude scaling ($d_{n50,Froude,model}$) - is larger than approximately 7mm the enlargement factor is given by

$$\frac{d_{n50,core,corr}}{d_{n50,core,Froude}} = 1.$$

Similar to the Reynolds scaling laws, this allows for a disregard of permeability similarity if the rocks size is large enough (Wolters et al., 2014).

Stability similarity

Lastly, to account for the difference in water density (fresh water models and salt water in coastal prototype settings) and rock density, stability scaling is used. Typically, this is done using the stability equation that was formulated using Hudson (1959)), namely: $W_{50} = \rho_r g H^3/(K_D \Delta^3 \cot\alpha)$. Stability similarity is assured when the stability number is equated for the model and the prototype, or

$$n_W = n_\rho \Big(\frac{n_L}{n_\Delta}\Big)^3.$$

Here n_W, n_ρ and n_Δ are the scale factor for the weight, density and relative density respectively, each defined similarly to equation (11).

4.2 Flume

The experiments are performed in a flume in the WaterLab of the faculty of Civil Engineering at the Delft University of Technology. The 2D wave flume that is used has a length of 39 metres, is 0.79 metres wide and 1 metre high. The flume is equipped with an electrical piston-type wave generator capable of producing regular and irregular wave fields with a significant wave height of up to 0.2 m. It is also equipped with active reflection compensation (ARC), which prevents the waves that are reflected by the structure in the flume to be re-reflected into the model by the wave board. To further ensure that the waves in the flume represent ones that occur in nature, second order wave steering is included in the wave board displacement calculations. Meaning that second order effects of the first higher and lower harmonics are accounted for. The structure is set-up at the far end of the flume, this guarantees that a 'deep water' section longer than five times the water depth is present between the wave paddle and the structure as suggested by Frostick et al. (2011). An overview of this an the location of wave gauges is given in figure 15. Information on the instrumentation, including that of the wave gauges can be found in Appendix D.

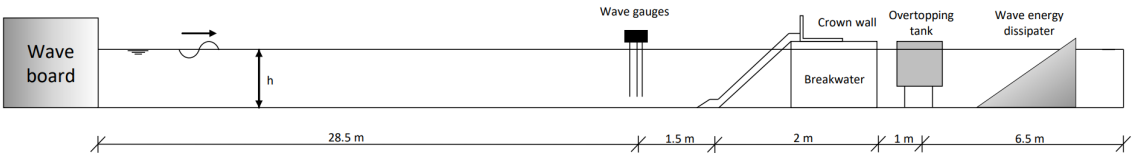

Figure 15: Full length overview of flume and experimental set-up.

4.3 Scale Model

A cross section of the scale model in the primary set-up is shown in figure 16. This section describes the design decisions and assumptions that have lead to this particular cross section. It also gives some insight into the constructions method.

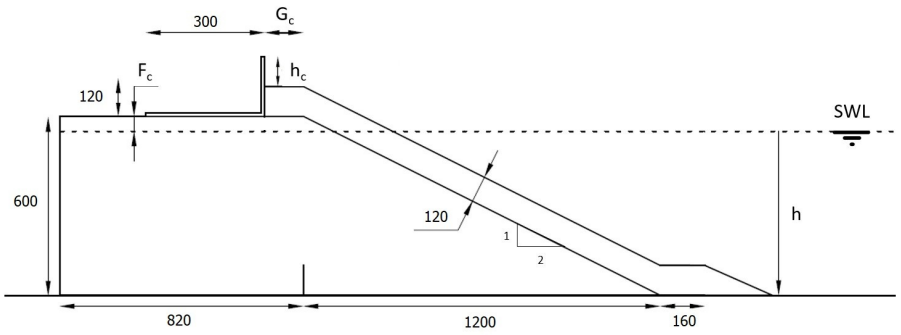

Figure 16: Cross section of breakwater and crown wall model with relevant parameters (in mm).

Breakwater

With the breakwater in figure 14 as a reference a prototype breakwater is designed. This breakwater has a typical slope of 1:2 at the front, which is somewhat gentler of a slope than shown in figure 14. This is done since a 1:2 slope is considered to be more general. The armour layer of the prototype is assumed to be 1-3 tons, with a core as per CIRIA (2007) (the grading of the prototype core can be found in Appendix B). Primarily using Froude scaling the model structure is designed, with a model scale of 17. Specifics of the scaling are expanded on in the remainder of this section.

The model structure has no rear slope since stability of the slope is not tested and because from a practical standpoint, having no slope is preferred and the lack of a typical rear slope is not expected to influence the measured output of this study. To allow for more data collection in the limited time, the breakwater is split in two parts by a wooden screen. This screen covers the full height and width of the breakwater to ensure that geometric differences between the two sides do not influence the hydraulic loading on either side.

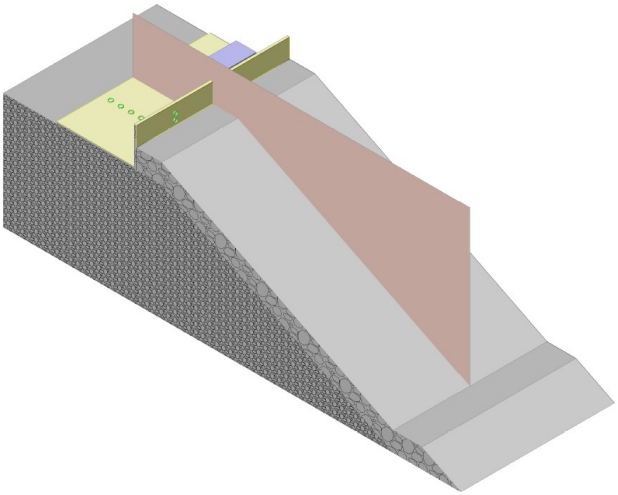

Figure 17: 3D rendering of the breakwater model, showing core and armour layer as well as wooden screen and crown walls with either pressure sensors or weights.

Armour

Using typical dimensions indicated by CIRIA (2007) chapter 6 (detailed in section 2.1), the slope of the core is armoured with a $2d_{n50}$ thick layer of rock (k_t assumed 1) with a width of 2.5 d_{n50} for the armour crest and $3d_{n50}$ for the toe. The nominal diameter of the armour rocks ($d_{n50} = 55.3mm$) is within the range as used in practice and based of the design equations as formulated by Van der Meer (1987) for the test conditions of this study (section 4.4). This nominal diameter sets the length scaling factor to 17, based on a typical 1-3 tons armour layer in the prototype. For the sake of simplicity the same rock as for the armour is used for the toe structure. This leaves it overdimensioned according to CIRIA (2007), but this is not expected to have an significant influence on the hydrodynamics around the crown wall.

After placement of the core in the flume, the armour layer is placed in-situ onto the core. To ensure the stability of the armour layer during the various tests, the stones are coated in epoxy before placement.

After construction of the armour layer, its (in situ) placement is validated using a laser scanner. In figure 18 the result of this scan can be seen. For four different cross sections the set-up is measured and analysed: two on either side of the dividing screen. This analysis indicates that the slope of the armour is 1:1.92 and the height of the unprotected part of the crown wall is $0.080m$. From this figure it also clear that a discrepancy between the base of the crown wall and the average core height is measured. This is the case because the rigid crown wall base will rest on the protruding rocks of the core. Since the foundation level is the most important water level parameter in this study, it is this value that is ensured to be accurate for the hydraulic conditions of each test. The water depth, as presented in section 4.4, gives a good estimation of the overall water depth in the flume, but it is not guaranteed in the whole flume (more on this in section 6).

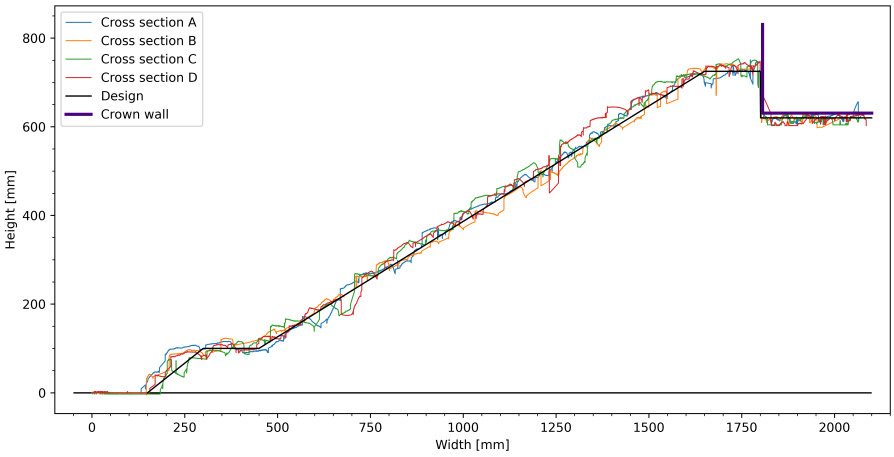

Figure 18: Four different cross sections as measured by laser scanner, for the set-up with armour crest width of 0.13m. The black line shows the design cross section and the coloured lines shown the measured ones.

Core

The core structure height is limited by the flume, as explained in section 4.1. The core material grading is the main parameter to be selected, and for this study, a general grading was chosen based on CIRIA (2007). This is a typical quarry run grading from which fines smaller than 100mm and oversized stones larger than 1m are removed (see Appendix B). The removal of fines improves the porosity of the structure and oversized stones can be repurposed for other parts of the structure, as is often done in practice. A scaled version ($n_L = 17$) of the grading was created for the model by blending four stone gradings and validated by weighing 500 stones from the mixture. The resulting grading curves can be found in Appendix B. The scaled version of the optimised core grading shown in Appendix B, has no rocks with a diameter smaller than 7mm, ensuring proper scaling for permeability as discussed in section 4.1.

Similarly to the armour, the core material is glued together using epoxy. Small quantities of rock at a time are mixed with epoxy using a concrete mixer and consequently dumped in a mould. This mould is fitted with a steel underplate and frame to allow for hoisting of the finished core in and out of the flume. To further improve the ease of hoisting the core is constructed from two separate pieces (each with its own mould), namely a triangular prism and a cuboid. Pictures that show this and the execution of can be found in Appendix **??**.

Crown wall

The base of the crown wall is chosen such that the shape of the pressure distribution can be measured in its entirety. That is to say that the length of the base is so long that the expected pressure at the last sensor is (close to) zero. The height of the vertical face is also taken to be somewhat larger than for the prototype as this also enables a better understanding of the pressure distribution and the difference between the protected and unprotected part. An overview of the sensor locations can be found in figure 19. A more detailed overview of the dimensions and sensor locations can be found in Appendix C.

The crown wall models are constructed from tricoya, as it is easy to work with and its exceptional lack of expansion when in contact with or submerged in water.

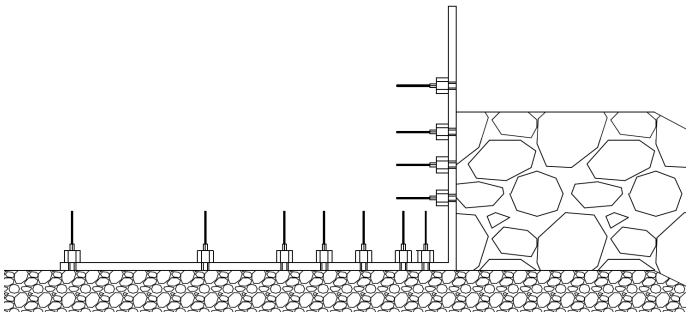

Figure 19: Cross section of crown wall model, showing the sensor locations.

4.4 Test conditions

The set-up was exposed to different test conditions to measure and test the relative importance and relation to wave height (H_s) and wave steepness (s_{0p}). Also, the set-up was adjusted to test the relative importance and relation for different geometric parameters. These parameters are the foundation level (F_c), crown wall height (d_c) and the armour crest width (G_c). From a single *base case* deviations are made in the geometry and hydraulic conditions to test how the change in that parameter translates to a change in the measured pressures and overall stability. Since the wave height and steepness are crucial parameters they are varied for every configuration of the test set-up. The ranges of the mentioned geometrical and wave condition variations can be found in table 6. For these configurations a test is done of one thousand waves. This wave record ensures statistical reliability and models a typical storm of a few hours in prototype scale, using a JONSWAP spectrum ($\gamma = 3.3, \sigma_a = 0.07$ and $\sigma_b = 0.09$).

Parameter	Range
H_s	0.125 - 0.175m
s_{0p}	0.015 - 0.04
$\xi_{m-1,0}$	2.37 - 3.87
d/L_{m0}	0.05 - 0.20
F_c/H_s	0 - 0.64
d_c/H_s	0.57 - 1.6
$G_c/d_{n50,armour}$	2.5 - 4

Table 6: Ranges of target wave conditions and structure dimensions for the breakwater model.

Pressure measurements

The main tests and output of this study is the temporal and spatial distribution of pressures along the crown wall for different breakwater configurations and wave conditions. A collection of twelve sensors is distributed over a single cross section of the crown wall. The distribution of these sensors is such that a good estimate of the horizontal wave impact can be made, but the focus and thus the majority of the sensors are used to measure a detailed pressure distribution along the wall base (see Appendix C). The crown wall is fixed to the structure to ensure that displacement of it will not influence the pressure readings.

Figure 20: Pressure sensors in base and face of fixed crown wall

Stability Tests

Model tests on overall stability are a staple in coastal engineering. They are used to validate design in specific context and geometry of a project. In this study they serve the main purpose of validating the stability criterion (as described in section 2.2). As the main pressure measurements rely heavily on the stability criterion for their applicability, a portion of the tests will focus on the overall stability and with it indirectly disprove or confirm the efficacy of the criterion. For these stability test the crown wall is not fixed, but instead the crown wall model is weight-down using weights. The crown wall, features a rectangular structure on its horizontal slab. This structure has been designed to hold steel plates securely in place and distribute their weight evenly across the width of the slab. The steel plates can be easily stacked within the structure, which is positioned to ensure that additional weight is added to the center of mass of the crown wall. Iteration is used with increasing weights to find the critical mass of the crown wall for varying wave conditions. This critical mass is the smallest mass for which the crown wall does not fail for a certain wave condition. Displacement of the crown wall indicates failure. This is measured using inductive proximity switches, where a displacement of $0.2mm$ or more qualifies as a failure. This is limits the displacement to less than half a centimeter in the prototype scale.

5 Data Analysis

5.1 Friction test

Using two different locations and two different crown walls, static friction coefficients for dry and wet conditions are found (see appendix D.5). To increase the confidence in the results, every variation is repeated ten times. The results can be found in table 7.

Crown element	Location	μ_{wet}	*St. Dev.*	μ_{dry}	*St. Dev.*
Element 1	#1	0.724	0.025	0.664	0.028
	#2	0.733	0.025	0.537	0.060
Element 2	#1	0.789	0.023	0.655	0.040
	#2	0.787	0.034	0.661	0.040
Average		**0.758**	**0.034**	**0.629**	**0.061**

Table 7: Friction coefficient for different conditions, with standard deviation

Typically, a friction coefficient of 0.5 is used for concrete elements placed on a rock core, as per CIRIA (2007). Bruun (2013), however, finds 0.7 as a representative value for field measurements. Moreover, using a similar breakwater and crown wall model, but with a different method Bekker et al. (2018) measured friction coefficients in the range of 0.67-0.74. These findings give confidence in the results as shown in table 7. For the remainder of this study the average value found for wet friction coefficient will be utilised, as for all wave conditions the interface between the crown wall and the core will be wet.

5.2 Stability tests

For the six base case wave conditions, multiple mass iterations were performed to determine the critical weight that just ensures stability of the crown wall. The results for the waves with a steepness of 4% are presented in Figure 21. The critical weight was determined as the average of the result of left and right side of the divider, with error bars indicating the uncertainty in the results. This uncertainty is dependent on the added mass due to overtopping and absorption, the discrepancy between the results on the left and right sides of the divider, and the step size used in the mass iteration.

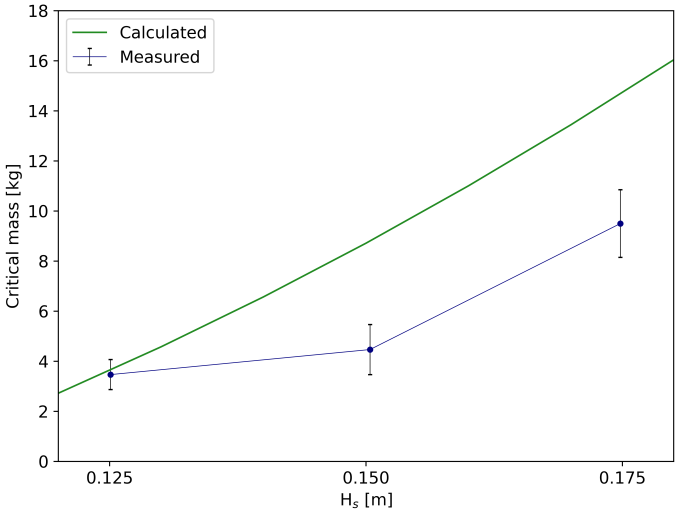

Figure 21: Mass of crown wall for which factor of safety is equal to 1 for varying wave height and a set wave steepness of 4%. The average is taken over the two sides of the flume divider.

The results from the experiment suggest a positive correlation between the critical mass and wave height, as shown in the graph. Interestingly, the expected critical mass as described by Bekker et al. (2018) in equation 8 also follows a similar trend to the measured results. However, the expected signal tends to overestimate the measured results. This discrepancy could be attributed to a few factors.

One important difference between this study and the one described by Bekker et al. (2018) is the mean armour and core stone diameter and distribution. The larger stones and smaller fines fraction used in this study make for a more porous breakwater. It could be expected that this decreases wave energy dissipation by the structure, resulting in a smaller critical mass. Crucially, this variance in the structure is not taken into account by the formulation from Bekker et al. (2018).

Another factor that could explain the discrepancy between the expected and measured signals is the height of the protruding part of the crown wall face. The smaller protruding part of the crown wall face used in this study allows for more overtopping and would be expected to result in lower forces on the crown element, resulting in smaller critical masses. However, Bekker et al. (2018) does not account for variations in the protruding crown wall height, which also raises questions about the general validity of equation 8.

5.3 Pressure signal analysis

Pressure sensor analysis

Preliminary analysis during testing showed ambiguous behaviour in the pressure signal. This was thoroughly investigated to increase the confidence in the results that are presented in the following sections. Two main patterns were identified, hereafter referred to as *slow decay* and *fast decay*. The fast decay is characterised by a non-physical, high pressure reading following a wave impact on the sensor, as is illustrated by the blue line in Figure 22 (for more see Figure 45). The pressure signal may suggest continued contact with water (droplets), but camera footage shows that after 0.4 seconds following the wave impact this is not the case. Lowering the excitation voltage from 10

to 2 volts and switching from a constant voltage to a constant current over the sensor has solved this particular undesired phenomenon.

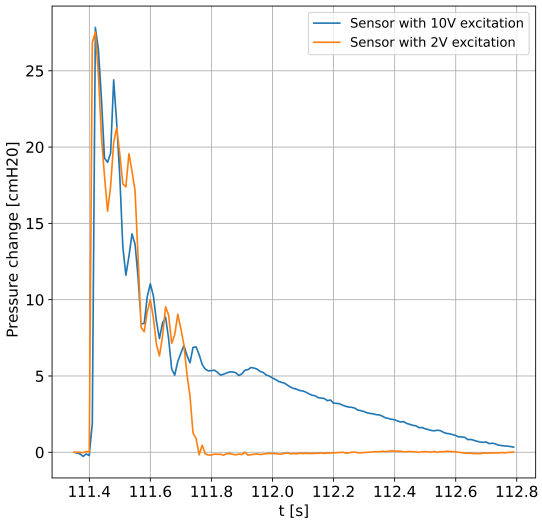

Figure 22: Pressure sensor with an excitation of 10 and 2 volts respectively, under comparable load. Both the fast decay phenomenon and the lack there of in the 2V sensor are clear.

The slow decay of the sensor is a phenomenon that can be most notably observed when the full sensor is submerged. After submersion, the sensor takes several minutes and up to two hours to go back to its reference value, which is a noticeable difference from the fast decay that occurs in the timescale of the wave period. However, the effect of slow decay is not much stronger than atmospheric perturbations that are expected to happen during these time frames. Since submersion of the whole sensor (both the sensing element and the casing) appear to correlate with this effect, it is not really noticeable for most tests where overtopping is limited. However, for tests with a lot of overtopping, the signal from the sensor needs to be filtered. This filtering is explained in the next section. More details on the sensor analysis can be found in Appendix E.

Pressure signal filter

A filter is applied to eliminate signal fluctuations that are unrelated to the wave impacts. This filtering is done by applying a moving mode filter to the signal of 1.1 times the peak wave period. The filter eliminates trends longer than a few wavelengths such as the slow decay phenomenon and since the pressure transducers are not vented it's also necessary to correct for atmospheric pressures changes. As a result, the filtered signal provides a more accurate representation of the wave impact pressure changes. Since the sensors are never submerged, the filter does not remove any constant pressure effects such as internal set-up and hydrostatic pressure.

Figure 23 demonstrates the operation of the filter for the critical wave in a test with a foundation level of zero. The blue line in the graph represents the raw signal after calibration, indicating the change in pressure. The red line depicts the moving mode for this signal, while the green line results from filtering, which essentially subtracts the red line from the blue line. As illustrated in the figure, the moving mode identifies the zero point just before every wave and employs it as a constant value throughout the incoming wave impact. For most sensors and tests the filter had

limited impact as the original signal was within 0.5 cmH20 of the expected value (unlike Figure 23).

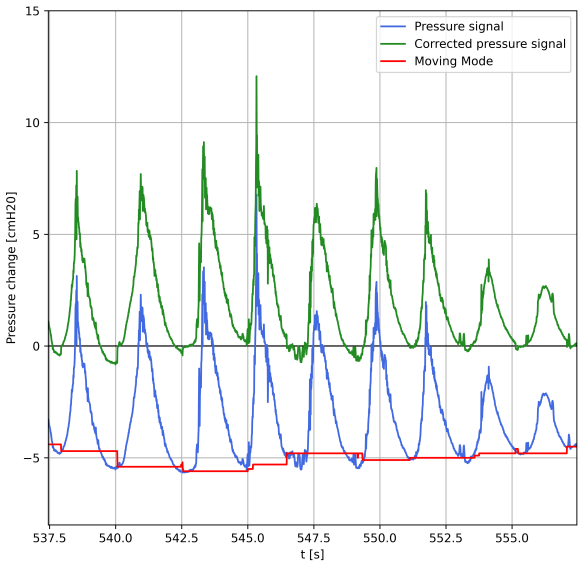

Figure 23: For the middle sensor in the crown wall base, the unfiltered, filtered and filter signal. The critical wave (545s) and others are shown for the test with $H_s = 0.15m$, $s = 2\%$ and $F_c = 0m$.

Pressure signal and distributions

The filtered pressure sensor data is analysed and presented in Figure 24. The figure displays the data for six sensors, which are located across the face and base of the structure, as depicted in the inset. It shows the pressure signal for the largest impact on the crown wall for the particular test. To improve the clarity of the graph, the individual sensor signals are smoothed using a moving mean of three data points, which is equivalent to 0.03s. The figure highlights that the largest pressures are the horizontal ones acting on the crown wall face. Additionally, these pressures are measured significantly earlier, providing preliminary evidence of the previously mentioned time lag between the horizontal and vertical forces acting on the crown wall.

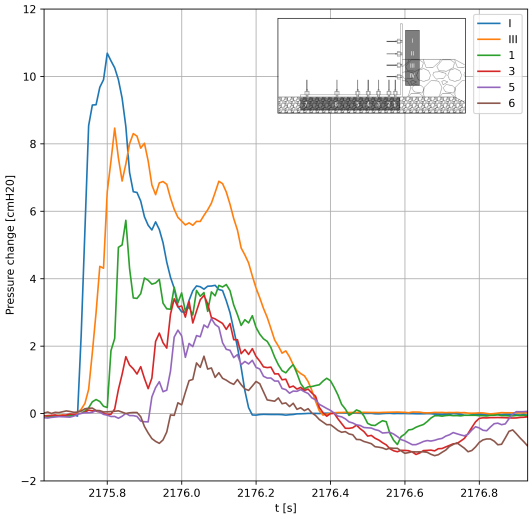

Figure 24: Temporal pressure distribution for a number of sensors on the face and base of the crown wall. The critical wave is shown for the test conditions: $H_s = 0.15m$, $s = 2\%$ and $F_c = 0.04m$

To improve understanding of the spatial distribution of these pressure during a critical wave, the pressures can also be plotted at their position along the crown wall. This visualisation is critical, since the description of the pressure distribution is an important part of literature (as highlighted in section 3). Thus, it is important to accurately describe this distribution. This study used point pressure measurements to approximate this distribution, which is illustrated in Figure 25. Each point on the graph represents the reading of a pressure transducer, with the grey open dots representing extrapolated values (which will be discussed further in the next section). It should be noted that the shown distribution is a snapshot captured during the biggest wave impact for a base case test. Figure **??** should show a animated figure showing the development of the pressure distribution during this critical wave impact (this function is supported by Adobe Acrobat, for individual stills the reader is referred to appendix F).

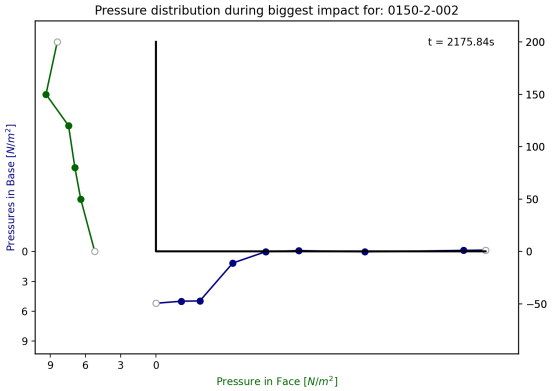

Figure 25: Crown wall pressure distributions along the face and base of the crown wall. The critical loading instance is shown for the test conditions: $H_s = 0.15m$, $s = 2\%$ and $F_c = 0.04m$

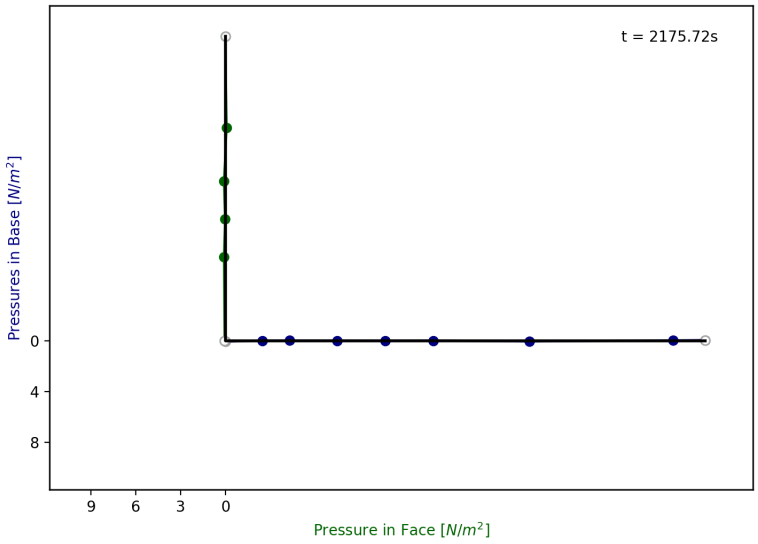

Figure 26: Animated graph of pressure distribution along the wall and base of the crown wall for the highest impact wave for $H_s = 0.150m$ and $s = 4\%$ and $F_c = 0.04m$.

For the instances of heaviest loading of the crown wall the vertical pressure distribution cannot be described by the triangle shape suggested by literature. Also, only a small part of the crown wall base is under vertical loading, much of the base is undisturbed by the wave. This is in contrary to the case of zero foundation level. In Figure 27 the biggest wave impact instance is shown for the same conditions as in Figure 25, with the sole difference of the foundation level. Here the suggested triangle shape can be clearly recognised and it would nicely describe the pressure distribution along the base of the crown wall.

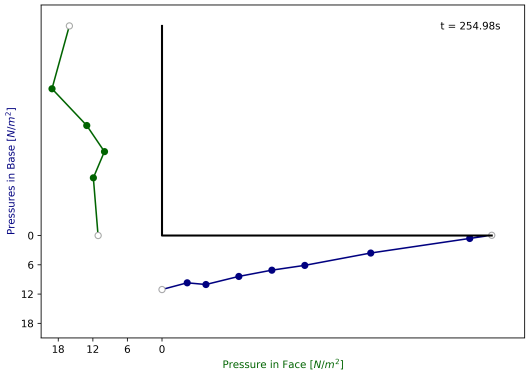

Figure 27: Crown wall pressure distributions along the face and base of the crown wall. The critical loading instance is shown for the test conditions: $H_s = 0.15m$, $s = 2\%$ and $F_c = 0.00m$

Figure 28 illustrates a more general picture for the relation that is just described, between the foundation level and the pressure distribution for the base of the crown wall. For each subfigure the six base case test conditions are combined to show a single mean pressure distribution and a local standard deviation. The sole difference between the subfigures is the indicated foundation level that is used in combination with the base case wave conditions. Figure 28c shows that the conclusion drawn for Figure 27 holds more generally, as it shows the same triangular shape and even a similar magnitude is measured for six tests with a variety of wave heights and wave steepnesses. Figure 28b shows that this triangular distribution does not in fact describe the pressure distribution for the base of the wall. Also, interestingly the magnitude of the pressure is significantly reduced. This is to be expected when considering that not the full amplitude of the wave but only a part of the top will reach the crown wall base. This effect is even stronger for the test conditions illustrated by Figure 28a. F_c/H_s in this case is approximately equal to the amplitude of the waves, which are thus expected to barely reach the crown wall base. Hence, the uplift pressures approach zero.

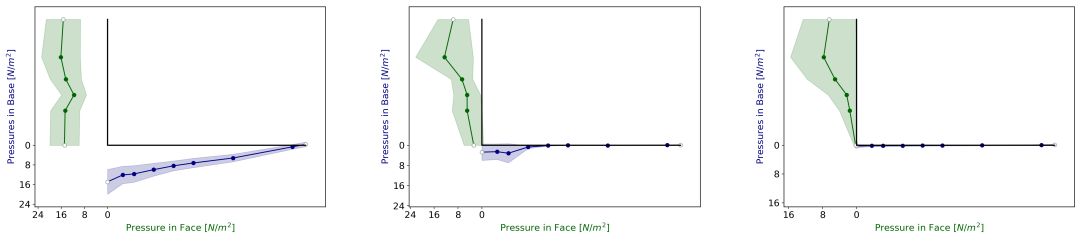

(a) $F_c/H_s = 0$ (b) $F_c/H_s \approx 0.25$ (c) $F_c/H_s \approx 0.50$

Figure 28: Pressure distribution average and standard deviation for three sets of tests for the same six wave conditions, for the critical wave in the test. Mean values are shown by the lines and each line is accompanied by the local value of the standard deviation.

5.4 Analysis of forces and factor of safety

Pressure extrapolation and integration

For a more complete description of the pressure distribution, three pressure points require extrapolation, namely the top of the face, the rear of the base, and the corner point. The decision-making

process surrounding extrapolation for these points is discussed here. For the point at the rear of the base linear extrapolation is deemed sufficient for determining the pressure, as both the extrapolation distance and the pressure here are relatively small. For the corner location, a weighted average is taken of the two linearly extrapolated values from the front and base of the crown wall based on the extrapolated distance to the corner. This method assumes a quasi-steady state and for the pressure in all directions to be the same for any point in the fluid, and the weighted average considers the relative confidence (based on its distance) in the extrapolations from the base and the face, respectively.

Various extrapolation methods were evaluated for the edge location at the top of the face, illustrated in 29. The first method assumes zero pressure, as during the maximum wave impact there is no water at the very top, so the local pressure is atmospheric. The second method uses linear extrapolation from the two closest sensors, which is a common approach but for this location it involves a relatively large distance of extrapolation. Lastly, the average of the two previous sensors is considered, which more closely resembles the expectations from literature that describes the pressure over the protruding part of the crown wall face to be constant (Martin et al. (1999), Pedersen (1996)).

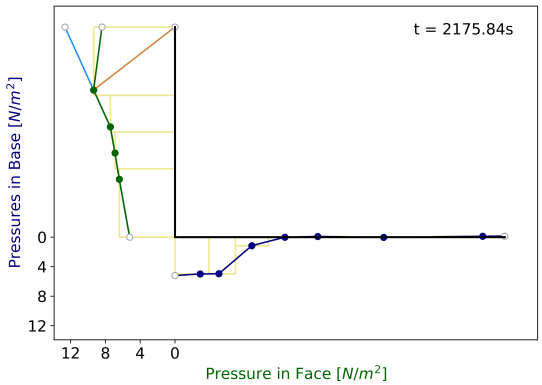

Figure 29: Different methods of force estimation from point pressure measurements on the crown wall. Grey open points show extrapolated values, with three options at the top of the face, namely extrapolated, averaged and zero for blue, green and orange respectively. The yellow boxes illustrate the Riemann sum for both the horizontal and vertical forces estimation.

To determine the best extrapolation method, all three methods are tested, and a sensitivity analysis is performed. The assumptions made in the tests include that each wave condition for each test is the critical one and the highest impact caused the structure to fail, the mass found in section 5.2 is the critical mass, and the factor of safety for that test is equal to one. This is done for all six base case tests for which both stability and a pressure measurements were done. The best extrapolation method is defined as the one with the minimum factor of safety closest to one during a particular test.

Moreover, a simple midpoint Riemann sum is used to estimate the forces on the element and compare them to the results obtained from different extrapolation methods. This method requires no extrapolation point, but instead takes the pressure point value for the area closest to the point in question, as illustrated in yellow in Figure 29. The results of the analysis are shown in table 8 for each individual test as well as the average minimal factor or safety and the mean square error per extrapolation method.

Test condition		Factor of Safety [-]			
Hs [m]	**s [-]**	**Riemann**	**Zero**	**Average**	**Extrapolate**
0.125	2	1.36	1.30	1.08	1.42
0.125	4	0.61	0.80	1.19	0.35
0.150	2	1.26	1.69	1.32	1.15
0.150	4	0.61	1.11	0.81	0.32
0.175	2	1.19	1.55	1.22	1.93
0.175	4	0.70	1.48	0.93	0.39
Average		0.95	1.32	**1.09**	0.93
MSE		0.11	0.19	**0.04**	0.39

Table 8: Extrapolation methods tests results, shown per test as well as mean and mean square error values per method.

It is assumed possible that different methods better describe the pressure distribution at different instances in a test. However, since the moment of smallest factor of safety is a crucial parameter in this study of stability, this instant is used to validate the right approach for the extrapolation. So, for the six base case tests, for which stability tests were performed, the different force calculation methods are compared on the basis of their lowest factor of safety in each test. In table 8 it can be seen that most methods have an mean value within 10% of the expected factor of safety (namely one). Taking into account the larger variance in the mean square error it is evident that the *average* method is the most suitable option. The Riemann sum closely resembles the *average* method, and therefore, it was expected that the results of the sensitivity analysis would be similar, which is confirmed by the analysis. However, the *average* method was ultimately chosen for two reasons, alongside the significantly lower MSE. Firstly, the *average* method is favoured because it has a stronger theoretical basis, as it is supported by the literature. Secondly, the *average* method ensures that the same pressure is taken for both the horizontal and vertical pressures at the corner point, as is expected for a quasi-steady state.

Lowest factor of safety

In the analysis of the results, the factor of safety plays a crucial role. However, calculating it requires the knowledge of the critical mass for each test condition, which is only known experimentally for the six base case test conditions. For the remaining tests, an iterative method is used to determine the critical mass. Specifically, the mass is iterated until the lowest factor of safety in each test is equal to 1. This assumes that all test conditions are critical. For each test a comparable plot to Figure 30 can then be created, showing the temporal distribution of the horizontal and vertical force and the factor of safety. It shows these values for the critical wave in this test, characterised by the drop in factor of safety to one. In it, three important instances can be defined, namely that of the highest horizontal force, the highest vertical force and the lowest factor of safety (all indicated by a cross in the figure).

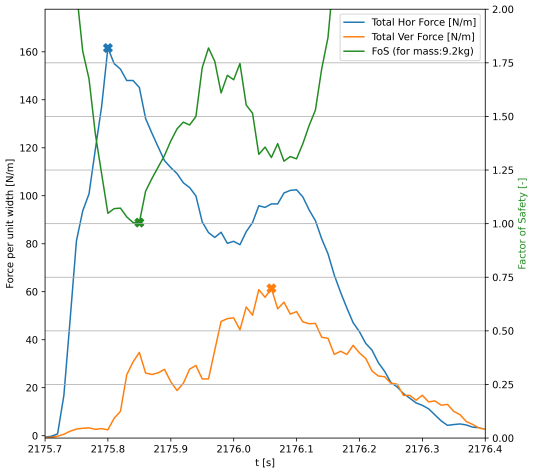

Figure 30: Horizontal and vertical force as well as factor of safety for the critical wave impact is shown for the test conditions: $H_s = 0.15m$, $s = 2\%$ and $F_c = 0.04m$. Crosses indicate the maximum value for the forces and the minimum value for the factor of safety in the range of this impact.

Figure 30 provides valuable insights into how the crown wall is loaded during wave impact and the consequences for its stability. One significant observation from the graph is the time lag between the maximum horizontal and maximum vertical forces. Furthermore, the graph shows the relative importance of horizontal and vertical forces on the crown wall's factor of safety and by extend, it's stability. The trend in the factor of safety appears to be strongly (negatively) correlated with that of the horizontal force force this wave condition. The graph also suggests that using the maximum horizontal and vertical force simultaneously as a design condition could be a quite conservative approach.

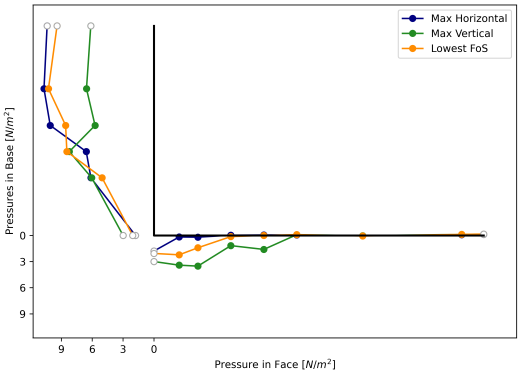

Figure 31: Crown wall pressure distributions along the face and base of the crown wall. Three lines represent the distributions for the instances of maximum horizontal and vertical force and minumun factor of safety for the critical wave for the test conditions: $H_s = 0.15m$, $s = 2\%$ and $F_c = 0.00m$

From Figure 30 it can be deduced that the horizontal and vertical forces, as well as the factor of safety, differ for each of the three defined instances. In addition to the magnitude of the forces, the spatial distribution of pressures can be illustrated, which provides further insights. Figure 31 depicts this distribution for the three instances discussed in Figure 30: maximum horizontal force, maximum vertical force, and minimal factor of safety. The lowest factor of safety should be taken into account for stability and design purposes, and thus, it can be compared to literature. The armour has a considerable impact on the reduction of pressures on the protected part of the wall face, in accordance with literature. It's also clear, however, that the vertical forces play a small role in the stability of the crown wall and are largely overestimated by current design methods for the instance of minimum factor of safety. The observation of reduced contact with water from Bekker et al. (2018) is also evident here, with more than half of the crown wall base having zero pressure readings for the highest vertical loading and even less for the other two instances.

Influence of foundation level

The loading characteristics of crown walls with different foundation levels show striking differences, as is already shown in Figure 28. To further illustrate this point, the six base case wave conditions are once again compared to the same conditions with a foundation level of zero and 0.08m, in Figure 32. The temporal distribution of forces and factor of safety for each critical wave impact was noted and normalized with the peak wave period of the respective test. Additionally, the horizontal and vertical forces were normalized with the maximum horizontal force of each critical wave impact. Normalizing both forces with the horizontal one maintains the relative importance and the overall shape of the temporal distribution as seen in Figure 30. These normalized values were averaged and the standard deviation was calculated for each set of six tests.

The resulting plots show the significant contrast in loading characteristics between the three sets of tests. Notably, the time lag between the maximum horizontal and vertical forces is significant when the foundation level is greater than zero, whereas for crown walls with a foundation level of zero, this time lag is practically non-existent. Moreover, in the latter case, the horizontal forces are only slightly smaller than the vertical forces, while in the former case, the vertical forces are a fraction of the horizontal forces, making them far less relevant for stability calculations. A possible explanation for this was given for Figure 28. It seems that the critical load for crown walls with

zero foundation level can be accurately described by the maximum vertical and horizontal force. However, for crown walls with a larger foundation level, the combination of maximum forces does not seem to represent the critical load well. Also, for the largest foundation level the vertical uplift appears barely significant.

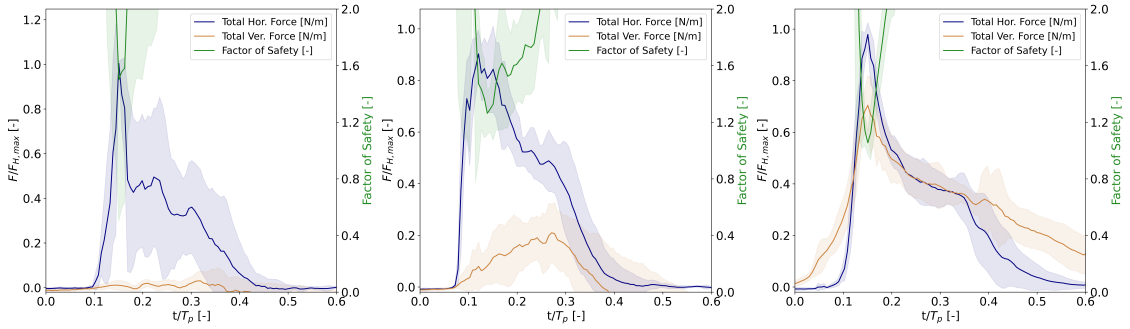

(a) $F_c/H_s = 0$ (b) $F_c/H_s \approx 0.25$ (c) $F_c/H_s \approx 0.50$

Figure 32: Three sets of tests results for the same six wave conditions, showing the normalised horizontal force, vertical force and factor of safety for the critical wave in the test. Mean values are shown by the lines and each line is accompanied by the local value of the standard deviation.

Figure 32 suggests a relationship between increasing foundation levels and the time lag between the largest vertical force and the moment of lowest safety factor. This relationship is made explicit in Figure 33, which plots the relative time lag (defined as the aforementioned time lag divided by the peak period of the specific test) against the dimensionless foundation level (F_c/H_s). The circles in this graph depict the same eighteen tests as in Figure 32. The open circles are excluded from the fit through the closed circles, as for the open circles the maximum vertical force is less than 5% of the maximum horizontal force and thus does not significantly influence stability. Comparing the six base case test for the three different foundation levels the correlation (shown in red) is clear and shows a convincing positive trend. It should, however, be noted that this correlation is less convincing when a variety of geometries are added to the analysis, as depicted with the open triangle and diamond shaped data points. Explaining this lack of strong correlation for a variety of geometries is complicated by the fact that these geometry variations are not tested for the other foundation levels. A possible explanation is that a more complex relation - taking into account the relative importance of these geometric variations - would better describe the relation between the time lag and foundation level.

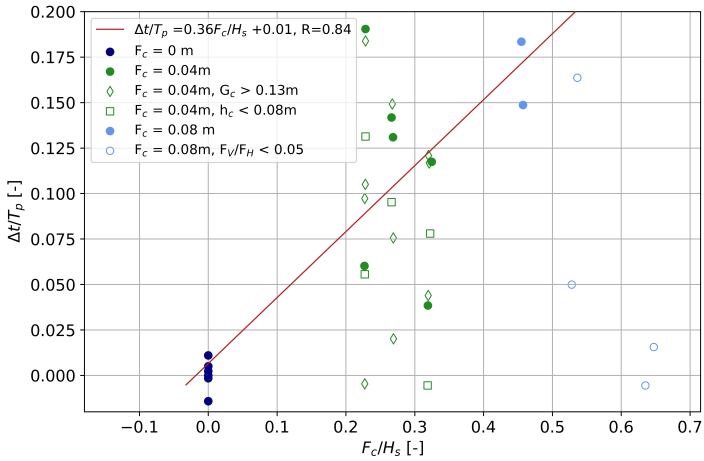

Figure 33: Relative time lag versus relative foundation level. Closed circles are the base case tests conditions for three different foundation levels and are used to fit the red line.

Not only the relative time lag can be plotted more explicitly but also the the ratio of the vertical force for these two time instances. This is done in Figure 34 which illustrates the ratio of the uplift force at the instance of minimum stability and the maximum uplift force during the wave impact of minimum stability, as a function of the relative foundation level. The closed circles represent the same six tests for three foundation levels as in Figure 32. However, as argued for Figure 33, some data points are excluded as the maximum vertical force is less than 5% of the maximum horizontal force and thus does not significantly influence stability. In addition, the open symbols represent the data points for geometries that vary from the base case.

The grey dashed line represents the fit through the closed circles, which indicates a clear negative correlation. The described ratio can be utilized as a correction factor for the time lag and associated lower but governing vertical force at the instance of minimum stability. This correction factor, denoted as γ_t, can be added to design methods that do not take this time lag into account. The red line in Figure 34 shows an adapted line that is slightly more conservative than the original fit. This line defines the formulation of the newly introduced reduction factor γ_t, which is defined as:

$$\gamma_t = \frac{F_{V,0.1\%,FoS}}{F_{V,0.1\%,max}} = -1.52\frac{F_c}{H_s} + 1.0 \tag{12}$$

It should be noted that this formulation is only valid within the parametric ranges as described in this study.

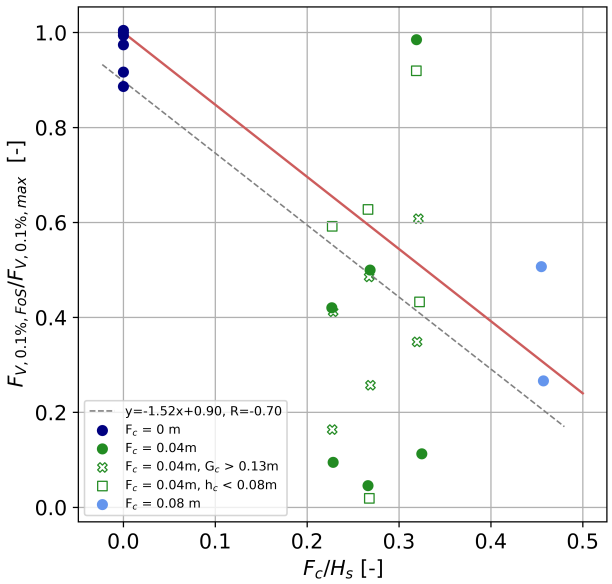

Figure 34: Ratio of lowest stability and maximum uplift pressure (separated in time by the aforementioned time lag) as a function of the relative foundation level. Closed circles show the base case tests conditions for three different foundation levels and are used to fit the grey line. Red shows the definition of the introduced factor γ_t.

5.5 Governing parameters in uplift pressures

In the preceding section of the paper, two distinct regimes were identified, based on the foundation level. The following section narrows the focus to the regime characterised by a foundation level greater than zero, given that the other parameters were varied for a foundation level of 0.04m (as shown in Figure 32b). Moreover, the study defined three distinct time instances in the previous section: that of the maximum horizontal force, the maximum vertical force, and the minimum factor of safety. Contrary to the previous analysis, here the instance of the maximum vertical force is chosen as the defining vertical force, so as to eliminate any dependence on the horizontal loads, which exists for the vertical force for the lowest factor of safety.

Statistical wave climate analysis

A thousand waves is often used as a typical number for a design storm. In this study so far, the maximum wave impact of a test has been studied, which for these thousand wave tests is the one in a thousand wave impact or 0.1% impact. This critical wave loading is crucial for stability calculations since it can be expected in a design storm. However, the drawback of using the 0.1% wave impact is that its analysis is hampered by coincidence, and the chance of an outlier is significant. To circumvent this issue, the focus of the continuation of this study will be on the tenth largest wave impact (the 1% wave impact) instead of the maximum wave impact. This allows for the study of extreme wave impacts with a reduced impact of coincidence in the data. Nevertheless, for stability, the largest wave impact or 0.1% wave impact is still crucial. Figure 35 shows a relation between the vertical forces for the 1% impact and the 0.1% impact, which exhibits a relatively stable ratio between the two forces. The slope in the trend line of this figure dictates

the constant conversion for the vertical force of the 0.1% impact from 1% impact data.

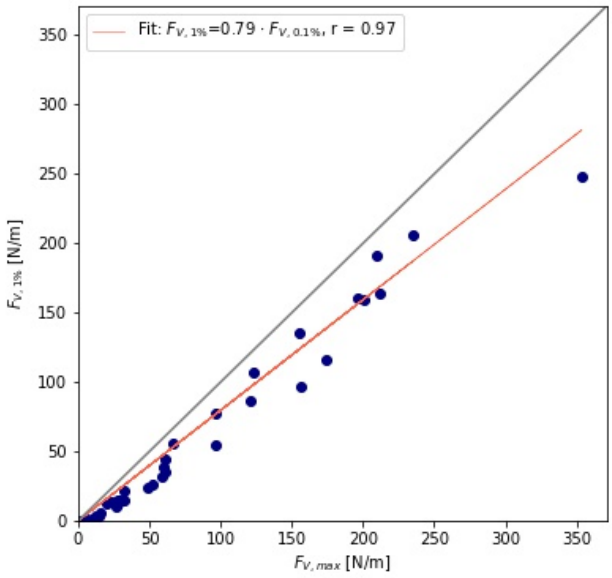

Figure 35: Comparison between vertical forces in critical wave ($F_{V,max}$) and forces exceeded by 1% the incident waves ($F_{V,1\%}$), for all tests.

Wave steepness

Figure 36 illustrates the 1% vertical forces for the base case geometry, with variations in wave height and wave steepness. The plot reveals a distinct pattern, showing a considerable and positive correlation between increasing wave height and decreasing steepness (or increasing wavelength) with the 1% uplift force. Taking into consideration that the less steep waves are longer and thus carry more water mass and with it momentum, it could be expected that for decreasing steepness there is an increase in uplift pressures.

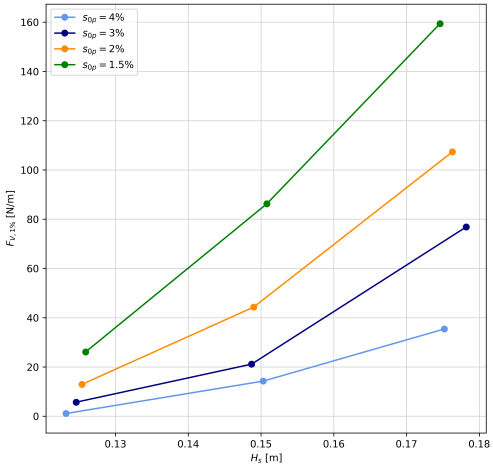

Figure 36: Largest vertical force for 1% wave impact versus wave height for varying wave steepness

Crown wall height

The correlation between the 1% uplift force, wave height, and wave steepness is further illustrated in graph 37. However, in contrast to the previous plot, this graph also shows the effects of changing the unprotected height of the crown wall. Since the uplift is calculated using pressure measurements on the horizontal base of the crown wall and not the vertical face, it could be expected that this variable would not have a clear correlation with uplift force and the graph confirms that it does not. In addition, the plot confirms the correlation shown in Figure 36 for different geometries.

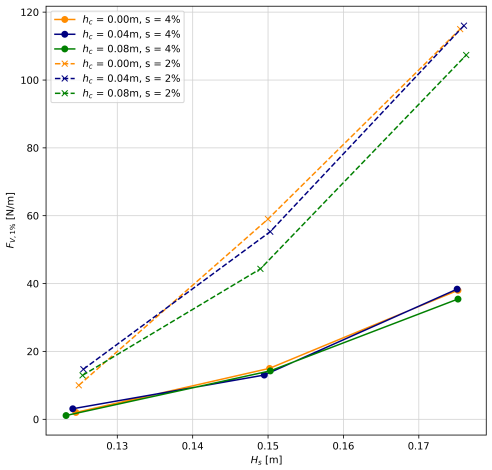

Figure 37: Largest vertical force for 1% wave impact versus wave height for varying crown wall protrusion height

Foundation level

The relationship between the 1% uplift force and the incident wave height is explored in Figure 38, which shows measurements for varying foundation levels. The importance of this variable cannot be overstated, as here again it is illustrated that changes in foundation level have a significant impact on the vertical force. The values for a foundation level of 0.08m are strikingly low. This can be attributed to the combination of water depth and wave height, where the peak of the incident wave has limited reach to the foundation of the crown wall, resulting in a little to no force exerted onto it. This effect diminishes for decreasing foundation level as expected as well.

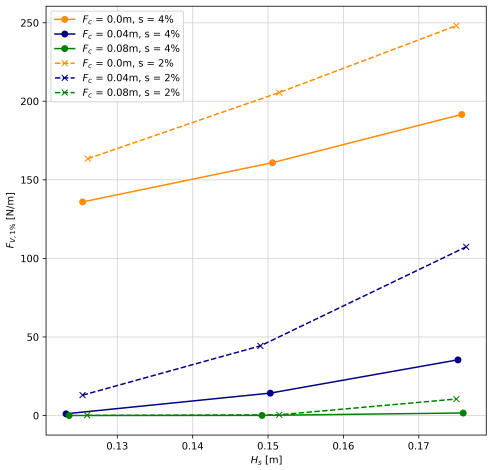

Figure 38: Largest vertical force for 1% wave impact versus wave height for varying foundation level

Armour crest width

In Figure 39 the uplift force versus wave height is shown for varying armour crest width. This larger armour crest seems to disproportionately affect the 4% waves. This is indicated by the fact that larger forces are measured for large crest widths with 2% waves than for small crest width with 4% waves. The magnitude of this effect seems to be larger (for the given parametric ranges) for increasing wave height, where all 2% waves (with varying Gc) exert a larger uplift force than the 4% waves. This could be explained by the fact that before a wave hits the crown wall base, its energy is dissipated by the armour first and then the core. Increasing the armour crest width directly increases the length over which the core can dissipate the wave energy of each wave before it hits the crown wall base, decreasing the wave's impact on it.

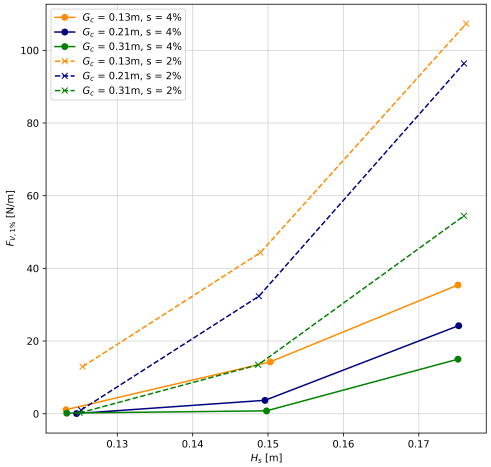

Figure 39: Largest vertical force for 1% wave impact versus wave height for varying armour crest width

5.6 Comparison to existing design methods

Pedersen (1996)

Figure 40 shows a comparison of the measured data with the expected ones as per Pedersen (1996) and Nørgaard et al. (2013) who proposed the triangular pressure distribution taken from the value of the pressure at bottom of the crown wall face. In the graph perfect alignment with the measured data is described by the grey line. In the graph the data points are group per foundation level. It is clear that Pedersen (1996) heavily overestimates the vertical forces, with an increasing overestimation for increasing foundation level. For the foundation level that was used for those test - namely 0m - the estimation is also too conservative but much better than for the other cases. This result does confirms findings by Bekker et al. (2018) that for increasing foundation level the estimations by this method are too conservative.

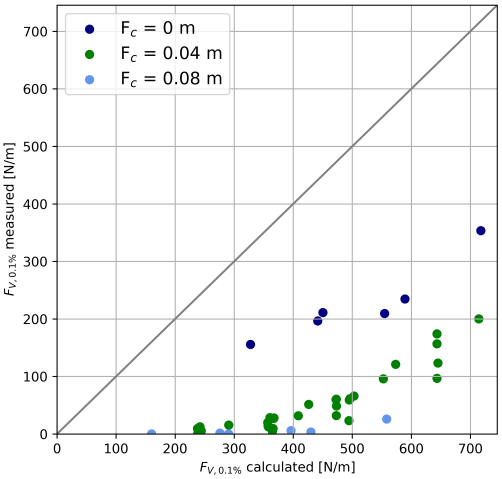

Figure 40: Measured versus expected vertical force (per Pedersen (1996)), grouped per foundation level.

6 Limitations

Set-up

After the breakwater structure was placed in the flume, it was observed that the alignment of the flume base was greatly influenced, likely due to the weight of the structure. This caused water depth variations of up to 2.5% to be measured both parallel and perpendicular to the wave direction. To mitigate the effect of this on the measurements, the water level in the flume is set by measuring the foundation level, as the foundation level is the most important water level parameter for this study. From this a representative value for the water depth in the flume is determined. This entails that for a particular wave the value of d/L_{0m} is not constant over the whole flume. However, since for all variations this value is in the intermediate water regime ($1/20 < d/L_{0m} < 1/2$) it is not anticipated that these effects would significantly affect the findings of this research.

Stability measurements

One oversight in this study was the lack of use of active reflection compensation (ARC) of the wave paddle movement during stability measurements (this is used for the pressure measurement tests), which compromises comparisons of the results to other methods such as Bekker et al. (2018). As the results of these tests play a crucial role in the analysis of extrapolation methods, this oversight also affects the rest of the study. However, since the extrapolation method with the smallest MSE is used instead of the closest mean, the pressure tests analysis is less affected by this issue. Moreover, the value of the critical mass deduced from the analysis serves only as an indication of the factor of safety, and is not expected to have influenced the definition of the critical wave.

Another limitation of the study is that the mass of the crown wall is not directly measured after each iteration, making it difficult to determine the precise mass that leads to failure or stability. Instead, estimates of the retained water on the crown wall, which increases the weight, and mass increase due to absorption are made. Additionally, for the largest wave conditions, a very large mass iteration spacing is used further decreasing the precision of these results.

Pressure sensor signal

While significant attention was given to ensuring proper pressure signals from the sensors, a few notes are necessary. Firstly, it was observed that the slow decay effect was most notable for submersion of the sensors, which was not much of a problem during testing but could impact the calibration process, which was done with submerged sensors. Nonetheless, a correlation factor of 1 or 0.99 for most sensors provides confidence in their proper calibration.

Also, the performance of the moving mode filter, which filters atmospheric perturbations and part of the slow decay, was examined for many different sensors, wave conditions, and test series points. However, it is practically impossible to verify if the filter is functioning correctly in all conditions. Notably, the filter may perform less effectively for very close wave groups or when a particular wave is quickly followed by another with little to no "zero" value in between. These conditions and their possible ramifications for the filter performance are exacerbated for the zero foundation level tests.

7 Conclusion and Recommendations

7.1 Conclusion

In this section the conclusions of this physical model study on the wave loads on emerged breakwater crown walls are summarized. This is done for each sub research question individually, and finally on the main research question.

How can uplift pressure distributions be described?

Conventional design methods rely on a triangular pressure distribution to model the vertical pressure on the base of the crown wall. However, this study has revealed that this approach is accurate, yet incomplete. The pressure distribution shape is irregular and inconsistent, and a triangular shape does not accurately represent the pressure for non-zero foundation levels. The analysis presented in this report demonstrates that, in general, there is a decrease in pressure from the front to the back of the base for most relevant wave load cases. However, large part of the base has a pressure of zero. For zero foundation level tests, the assumption from literature holds, and a clear triangular shape accurately describes the vertical pressure distribution over the base of the crown wall. Also, for conditions where F_c/H_s exceeds 0.5 uplift pressure is expected to influence the stability of the structure.

Do time lags between horizontal and vertical maximum pressures occur and how can they be included in a design method?

Similar to the pressure distribution this study has shown that there are distinct differences in wave load characteristics for zero and non-zero foundation level wave conditions. For zero foundation level conditions, the maximum horizontal force, maximum vertical force, and minimum factor of safety align perfectly in one instance, and there is no time lag. However, for increasing foundation level conditions, a clear time lag can be identified. A linear positive relation between the relative time difference and relative foundation level is found. These relative time lags ($\Delta t/T_p$) are in the order of 0.1-0.2 [-]. For various geometric and wave condition variations, the time lag is substantial enough to necessitate its inclusion in stability considerations, the difference in vertical force between these two instances is significant. A reduction factor (γ_t) for the vertical force for stability calculations is introduced that can be used to take these time lags in to account.

What parameters are governing in estimating uplift pressures?

This report includes numerous figures illustrating the influence of various parameters on the vertical loading of breakwater crown walls. Across many different geometries and wave conditions, the study investigated the effects of wave height and wave steepness. The analysis revealed that wave height is strongly positively correlated with the vertical forces, while steepness is negatively correlated with it, with longer waves are associated with larger vertical forces.

Furthermore, the study demonstrated that the foundation level has a crucial influence on the vertical forces. Even a relatively small variation of the foundation level, equivalent to a fraction of the wave height, has a tremendous impact on the vertical loads. The investigation concluded that for a relative foundation level higher than 0.5 no significant uplift pressure are present.

The study also tested the variation of the armour crest width, revealing a strong negative correlation with the vertical forces on the crown wall. For the tested range, the impact on the vertical forcing even seems to dominate over the effect of wave steepness.

Finally, the height of the crown face was investigated, but no clear correlation was identified with the vertical forces.

Can the use of estimates of wave overtopping improve estimates of wave loads?

In this study, the proposal to use overtopping as a force estimator is called into question. Despite its prevalence in contemporary literature, the proposal is not experimentally tested due to its apparent incoherence. Specifically, the use of a mean parameter to estimate extreme forces is called into question. Additionally, the proposal is contradicted by the finding that a lower crown wall would result in larger overtopping and smaller forces, highlighting incoherence of this method.

Can current design methods for force estimations on crown walls be improved in their description of relevant phenomena and relation between wave conditions and horizontal and vertical forces on crown walls?

This study investigates the estimation of uplift pressures on breakwater crown walls. The study reveals that the conventional design methods based on a triangular pressure distribution is accurate but incomplete. This shape does not accurately represent non-zero foundation levels. The study also shows a time lag between horizontal and vertical maximum pressures, which must be considered in stability considerations for non-zero foundation level wave conditions. The influence of various parameters on vertical loading, such as wave height, steepness, foundation level, and armour crest width, is investigated, and their correlation with vertical forces is revealed. The importance of taking foundation level and armour crest width into consideration is highlighted. The proposal to use overtopping as a force estimator is rejected.

7.2 Recommendations

Sensor placement

The analysis of the pressure distribution and estimation of total forces on the crown wall base and face can be improved through various means. One suggestion is to increase the density of pressure point measurements by adding more sensors. Another option is to improve the spacing of existing sensors by placing edge sensors closer to the edge, reducing extrapolation distances and associated uncertainties. Additionally, sealing the sensor casings from exposure to water could further enhance the set-up. This would also eliminate the effect of the slow decay phenomenon, which could be completely disregarded with an additional isolation barrier around the sensors. These improvements could lead to more accurate measurements and a better understanding of the pressure distribution and forces acting on the crown wall.

Foundation level

This study proposes the use of two distinct regimes to describe the vertical forces and stability for zero and non-zero foundation levels. The aim of this approach is to accurately capture the behaviour of the breakwater crown wall under different wave conditions and geometries. However, it is suggested that elaborate testing for more closely spaced intervals of foundation levels could provide a better (continuous) description of the vertical forces in a variety of foundation levels. This approach could potentially lead to an improved understanding of the behaviour of the breakwater crown wall and contribute to more accurate design methods.

Numerical simulations

A potential avenue for further exploration of the objectives outlined in this report is the use of a numerical model. The calibration of such a model could be conducted utilising the data set from this study. Subsequently, a vast range of variables and intervals could be analyzed using this calibrated model to gain a more detailed understanding of their influence. The results could be

further refined by testing smaller variation intervals and examining a wider range of variables and different variables.

Continuation with this data set

Continued analysis of the data set from this study could provide valuable insights into the accuracy and applicability of existing methods for non-zero foundation levels. In particular, analysis of methods other than that of Pedersen (1996) could lead to a better understanding of their performance under the specific hydraulic and geometrical conditions studied here, with an emphasis on non zero foundation level.

Furthermore, some conclusion in this report are based on only a handful of tests in this study. Further persistence might result in more generalised conclusions, applicable in a large range of geometries and hydraulic conditions. Continuation of this analysis could also yield improvements of these aforementioned other design methods and/or yield a new design method all together.

References

Aniel-Quiroga, I., Vidal, C., Lara, J. L., & Gonzalez, M. (2019). Pressures on a rubble-mound breakwater crown-wall for tsunami impact. *Coastal Engineering*, *152*, 103522.

Battjes, J. A. (1974). Surf similarity. In *Coastal engineering 1974* (pp. 466–480).

Bekker, J., Hofland, B., & Smith, G. (2018). Experiments on the effect of freeboard on the stability of a breakwater crown wall. *Coastal Engineering Proceedings*(36), 9–9.

Bruun, P. (2013). *Design and construction of mounds for breakwaters and coastal protection*. Elsevier.

Cecioni, C., Franco, L., & Bellotti, G. (2019). Wave forces on breakwater crown walls: physical model tests and improvement of prediction. *Coastal Structures 2019*, 314–323.

CIRIA. (2007). *The rock manual. the use of rock in hydraulic engineering (2nd edition)*. C683, CIRIA, London.

Fennell, P. S., Davis, S. J., & Mohammed, A. (2021). Decarbonizing cement production. *Joule*, *5*(6), 1305–1311.

Franco, L., Bellotti, G., & Cecioni, C. (2018). Physical model tests of wave overtopping and forces on breakwater crown walls. *Coastal Engineering Proceedings*(36), 63–63.

Frostick, L., McLelland, S. J., Mercer, T. G., et al. (2011). Users guide to physical modelling and experimentation. *IAHR design manual*.

Group, D. (n.d.). *Hanstholm port: Fighting north sea waves.* Retrieved from `https://www.dhigroup.com/global/references/emea/overview/hanstholm-port-fighting-north-sea-waves`

Hamilton, D. G., & Hall, K. R. (1993). Preliminary analysis of the stability of rubblemound breakwater crown walls. In *Coastal engineering 1992* (pp. 1217–1230).

Han, X., Jiang, Y., & Dong, S. (2022). Wave forces on crown wall of rubble mound breakwater under swell waves. *Ocean Engineering*, *259*, 111911.

Heller, V. (2011). Scale effects in physical hydraulic engineering models. *Journal of Hydraulic Research*, *49*(3), 293–306.

Hudson, R. Y. (1959). Laboratory investigation of rubble-mound breakwaters. *Journal of the waterways and Harbors division*, *85*(3), 93–121.

Jensen, O. J. (1984). *A monograph on rubble mound breakwaters*. Danish Hydraulic Institute.

Losada, M. A., & Dalrymple, R. A. (1993). Water waves on crown breakwaters. *Journal of waterway, port, coastal, and ocean engineering*, *119*(4), 367–380.

Losada, M. A., & Gimnez-Curto, L. A. (1980). Flow characteristics on rough, permeable slopes under wave action. *Coastal Engineering*, *4*, 187–206.

Martin, F. L., Losada, M. A., & Medina, R. (1999). Wave loads on rubble mound breakwater crown walls. *Coastal Engineering*, *37*(2), 149–174.

Molines, J., Herrera, M. P., & Medina, J. R. (2018). Estimations of wave forces on crown walls based on wave overtopping rates. *Coastal Engineering*, *132*, 50–62.

Molines, J., & Medina, J. R. (2016). Explicit wave-overtopping formula for mound breakwaters with crown walls using clash neural network–derived data. *Journal of Waterway, Port, Coastal, and Ocean Engineering*, *142*(3), 04015024.

Molines, J., & Medina, J. R. (2019). Crown wall stability of cube and cubipod armored mound breakwaters. *Coastal Structures 2019*, 3–9.

Negro Valdecantos, V., López Gutiérrez, J. S., & Polvorinos Flors, J. I. (2013). Comparative study of breakwater crown wall–calculation methods. In *Proceedings of the institution of civil engineers-maritime engineering* (Vol. 166, pp. 25–41).

Nørgaard, J. Q. H., Andersen, T. L., & Burcharth, H. F. (2013). Wave loads on rubble mound breakwater crown walls in deep and shallow water wave conditions. *Coastal Engineering*, *80*, 137–147.

Pedersen, J. (1996). Wave forces and overtopping on crown walls of rubble mound breakwaters: an experimental study.

Smolka, E., Zarranz, G., & Medina, J. (2009). Estudio experimental del rebase de un dique en talud de cubípodos. *Libro de las X Jornadas Españolas de Costas y Puertos*, 803–809.

Steendam, G. J., van der Meer, J. W., Verhaeghe, H., Besley, P., Franco, L., & van Gent, M. (2005). The international database on wave overtopping. In *Coastal engineering 2004: (in 4 volumes)* (pp. 4301–4313). World Scientific.

Van den Bos, J., & Verhagen, H. (2018). Breakwater design. *Delft University of Technology*.

Van der Meer, J. W. (1987). Stability of breakwater armour layers—design formulae. *Coastal engineering*, *11*(3), 219–239.

Van der Meer, J. W., & Stam, C.-J. M. (1992). Wave runup on smooth and rock slopes of coastal structures. *Journal of waterway, Port, coastal, and Ocean Engineering*, *118*(5), 534–550.

van Gent, M. (1995a). Porous flow through rubble-mound material. *Journal of waterway, port, coastal, and ocean engineering*, *121*(3), 176–181.

van Gent, M. (1995b). Wave interaction with permeable coastal structures.

van Gent, M. R., van den Boogaard, H. F., Pozueta, B., & Medina, J. R. (2007). Neural network modelling of wave overtopping at coastal structures. *Coastal engineering*, *54*(8), 586–593.

Van Heemst, C. (2014). *Stability of a crown wall on a breakwater: A refinement of existing design formulae* (Unpublished doctoral dissertation). Delft University of Technology.

Verhaeghe, H., Van der Meer, J., Steendam, G.-J., Besley, P., Franco, L., & Van Gent, M. (2004). Wave overtopping database as the starting point for a neural network prediction method. *Coastal Structures 2003*, 418–430.

Wenneker, I., & Hofland, B. (2014). Optimal wave gauge spacing for separation of incoming and reflected waves. In *Proc., 5th int. conf. coastlab 14, application of physical modelling to port an coastal protection.*

Wolters, G., van Gent, M., Allsop, W., Hamm, L., & Muhlestein, D. (2010). Hydralab iii: Guidelines for physical model testing of rubble mound breakwaters. In *Coasts, marine structures and breakwaters: Adapting to change: Proceedings of the 9th international conference organised by the institution of civil engineers and held in edinburgh on 16 to 18 september 2009* (pp. 559–670).

Wolters, G., Van Gent, M., Hofland, B., & Wellens, P. (2014). Wave damping and permeability scaling in rubble mound breakwaters. In *Proc., 5th int. conf. on the application of physical modelling to port and coastal protection, coastlab14* (pp. 1–11).

A Test conditions

#	$\mathbf{H}_s$ [m]	$\mathbf{T}_p$ [s]	h [m]	$\mathbf{F}_c$ [m]	$\mathbf{G}_c$ [m]	$\mathbf{h}_c$ [m]	Type
1	0.125	1.55	0.56	0.04	0.13	0.20	
2	0.150	1.67	0.56	0.04	0.13	0.20	
3	0.175	1.41	0.56	0.04	0.13	0.20	**Base Case**
4	0.125	2.00	0.56	0.04	0.13	0.20	test conditions
5	0.150	2.19	0.56	0.04	0.13	0.20	
6	0.175	2.37	0.56	0.04	0.13	0.20	
7	0.150	1.79	0.56	0.04	0.13	0.20	
8	0.175	1.93	0.56	0.04	0.13	0.20	
9	0.125	1.63	0.56	0.04	0.13	0.20	Steepness variation
10	0.150	2.53	0.56	0.04	0.13	0.20	$s = 1.5\&3\%$
11	0.175	2.73	0.56	0.04	0.13	0.20	
12	0.125	2.31	0.56	0.04	0.13	0.20	
13	0.150	1.55	0.52	0.08	0.13	0.20	
14	0.175	1.67	0.52	0.08	0.13	0.20	
15	0.125	1.41	0.52	0.08	0.13	0.20	
16	0.150	2.19	0.52	0.08	0.13	0.20	
17	0.175	2.37	0.52	0.08	0.13	0.20	
18	0.125	2.00	0.52	0.08	0.13	0.20	Foundation level variation
19	0.150	1.55	0.60	0.00	0.13	0.20	$F_c = 0$ &$0.08m$
20	0.175	1.67	0.60	0.00	0.13	0.20	
21	0.125	1.41	0.60	0.00	0.13	0.20	
22	0.150	2.19	0.60	0.00	0.13	0.20	
23	0.175	2.37	0.60	0.00	0.13	0.20	
24	0.125	2.00	0.60	0.00	0.13	0.20	
25	0.150	1.55	0.55	0.04	0.31	0.20	
26	0.175	1.67	0.55	0.04	0.31	0.20	
27	0.125	1.41	0.55	0.04	0.31	0.20	
28	0.150	2.19	0.55	0.04	0.31	0.20	
29	0.175	2.37	0.55	0.04	0.31	0.20	
30	0.125	2.00	0.55	0.04	0.31	0.20	Armour crest width variation
31	0.150	1.55	0.55	0.04	0.21	0.20	$G_c = 0.31$ & $0.21m$
32	0.175	1.67	0.55	0.04	0.21	0.20	
33	0.125	1.41	0.55	0.04	0.21	0.20	
34	0.150	2.19	0.55	0.04	0.21	0.20	
35	0.175	2.37	0.55	0.04	0.21	0.20	
36	0.125	2.00	0.55	0.04	0.21	0.20	
37	0.150	1.55	0.55	0.04	0.13	0.15	
38	0.175	1.67	0.55	0.04	0.13	0.15	
39	0.125	1.41	0.55	0.04	0.13	0.15	
40	0.150	1.55	0.55	0.04	0.13	0.15	
41	0.175	2.37	0.55	0.04	0.13	0.15	
42	0.125	2.00	0.55	0.04	0.13	0.15	Crown wall height variation
43	0.150	2.19	0.55	0.04	0.13	0.10	$h_c = 0.15$ & $0.10m$
44	0.175	1.67	0.55	0.04	0.13	0.10	
45	0.125	1.41	0.55	0.04	0.13	0.10	
46	0.150	2.19	0.55	0.04	0.13	0.10	
47	0.175	2.37	0.55	0.04	0.13	0.10	
48	0.125	2.00	0.55	0.04	0.13	0.10	

B Sieving Curves for breakwater rock gradings

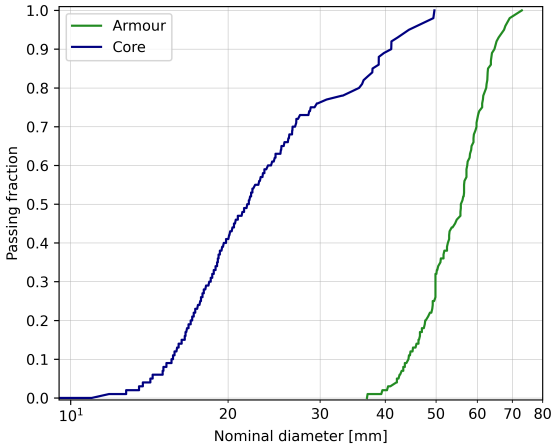

Figure 41: Sieving curve for both armour and core rocks, based on 500 samples each.

	Nominal diameter [mm]	
Passing fraction	**Armour**	**Core**
0.10	43.9	15.8
0.15	45.8	16.5
0.50	55.3	22.1
0.60	56.8	23.6
0.85	61.8	36.5

C Crown wall design, dimensions and sensor location

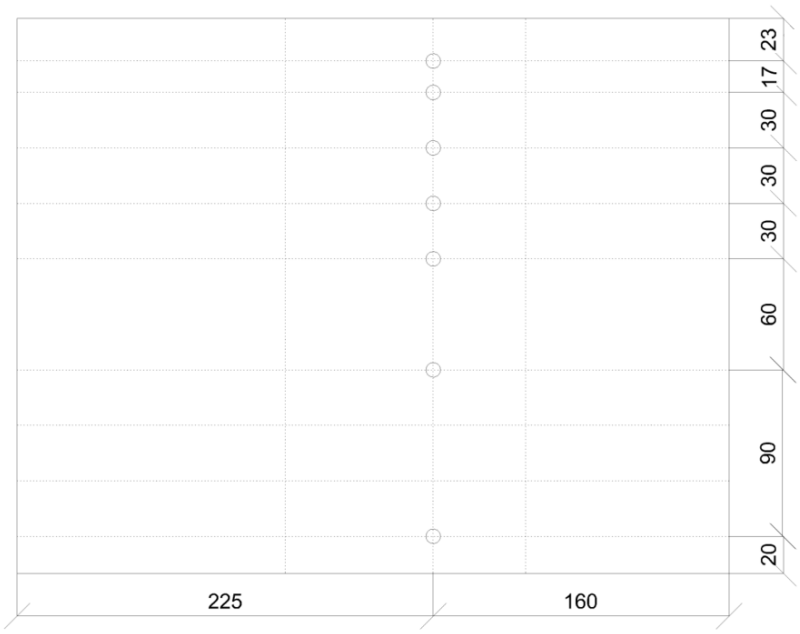

Figure 42: Dimensions of crown wall base; top view showing sensors location as circles.

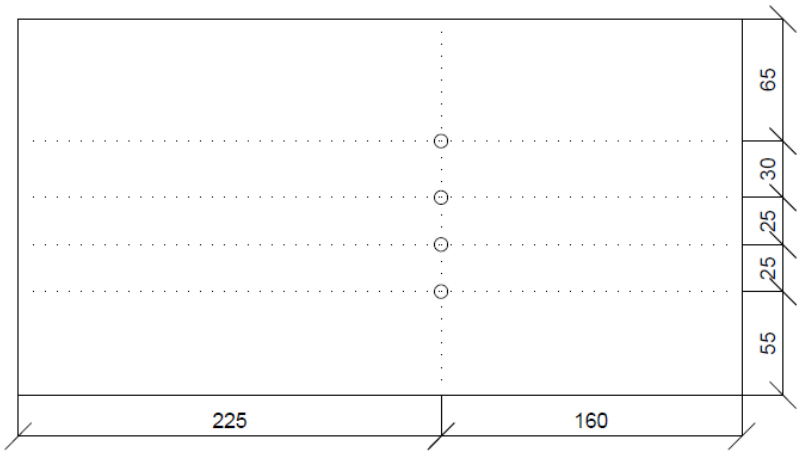

Figure 43: Dimensions of crown wall face; Front view showing sensors location as circles.

D Instruments

A range of different sensors and instruments have been used to gather data that either confirms the set-up is working as intended or details the necessary output to verify the validity of the hypothesis that are tested in this study. The analog output signal (a value between -10 and 10 volts) of these sensors is fed to a computer equipped with DaisyLab data acquisition and analysis software. This raw data (a signal of a variable voltages in time) is translated into the relevant units using carefull calibration and Python.

D.1 Laser scanner

As an important step in validating if the structure is constructed as intended a laser scanner is used. The combination of a laser on a cart with a pulse wheel can give a detailed profile of a transect of the structure. The cart is mounted on wheels that can roll over rails on top of the flume and an extra wheel that measures its own rotation is part of the laser scanner device. A compact laser triangulation displacement sensor is also mounted on the cart. The laser provides a precise value for the vertical displacement (relative distance between the laser and the armour layer), while the pulse wheel provides the horizontal displacement.

D.2 Wave gauge

To confirm that the incident wave conditions for each test match the desired conditions, several wave gauges are deployed. These submerged probes measure the water column through changes in conductivity. Since significant parts of the wave energy will be reflected by the structure, the reflected and incoming parts of the wave signal should be separated. This is accomplished by the use of three probes which are spaced appropriately. For any set of wavelengths there is an optimal relative spacing of the three probes as proposed by Wenneker & Hofland (2014). The DECOMP-tool from the TU Delft Waterlab is used to do the wave analysis and determine the wave conditions of each test. In this study a set of three gauges is arranged near the toe of the structure but far enough away to reduce the effect from evanescent modes (Frostick et al., 2011). These gauges are placed such that they accommodate a 30-40 separation as is standard practice in the WaterLab. Additionally, three more probes (30-40) are placed at a few wavelengths from the wave generator. An overview of this set-up can be found in figure 15

D.3 Rangefinder

To test horizontal and vertical displacement for the stability tests, proximity sensors are placed at the rear and the top of the crown element respectively. The accuracy of the sensors is in the range of 0.02mm at a sample rate of 100Hz.

D.4 Pressure transducer

To acquire data on the temporal en spatial distribution of pressure over the base and face of the crown wall, high-end pressure sensors are used, namely Kulite's HKM-375M. These unvented pressure transducers have a pressure range of 1 bar and use a flush metal diaphragm as a force collector. The pressures are measured at 100 Hz, which allows for similar results when compared to higher frequencies (Han et al., 2022). The arrangement of the sensors can be found in Appendix C).

D.5 Friction test setup

To accurately apply the stability criterion as described in section 2.2 the friction coefficient μ needs to be assessed. Using a sample of the core rocks hinged to a base, the set-up can be tilted and the angle for which the crown wall mobilises can be found.

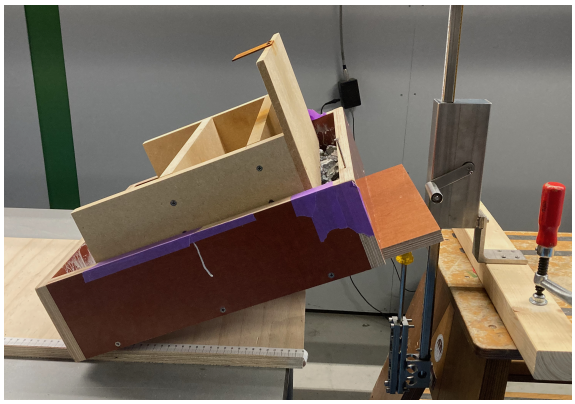

Figure 44: Set-up used for studying wet and dry static friction.

E Extended sensor analysis

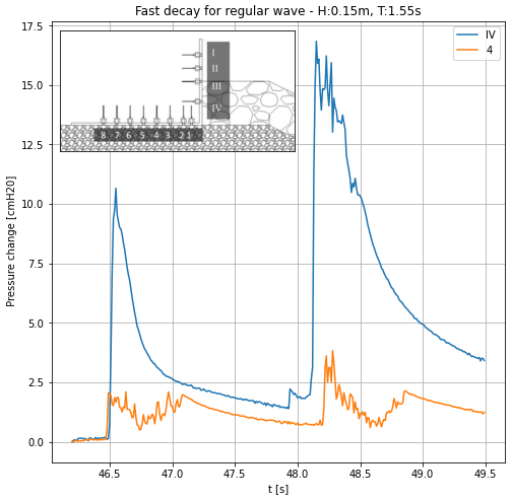

Figure 45: Fast decay phenomenon of a sensor in the vertical and horizontal slab of the crown wall. The inset shows the location of the two sensors in the crown wall.

F Time laps of pressure distributions

.

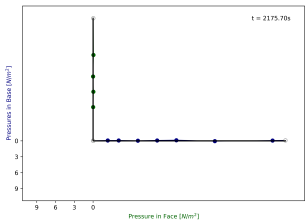

(a) Timestamp: 2175.70s

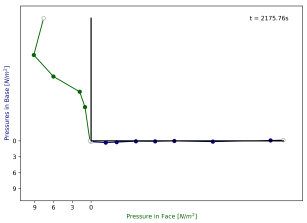

(b) Timestamp: 2175.76s

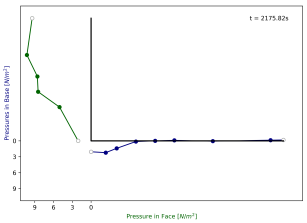

(c) Timestamp: 2175.82s

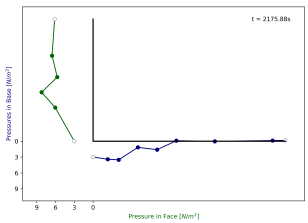

(d) Timestamp: 2175.88s

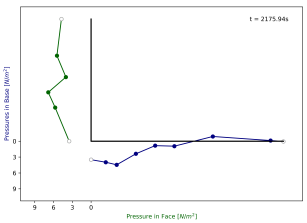

(e) Timestamp: 2175.94s

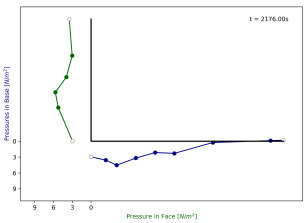

(f) Timestamp: 2176.00s

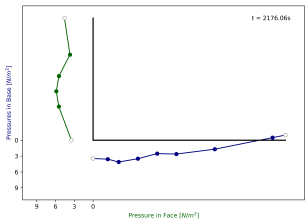

(g) Timestamp: 2176.06s

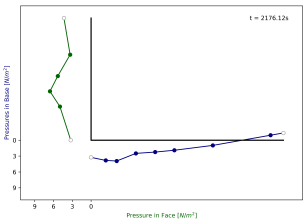

(h) Timestamp: 2176.12s

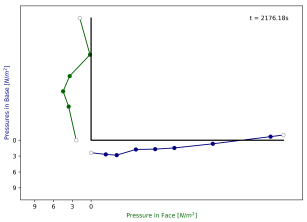

(i) Timestamp: 2176.18s

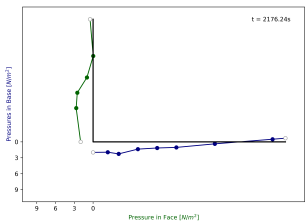

(j) Timestamp: 2176.24s

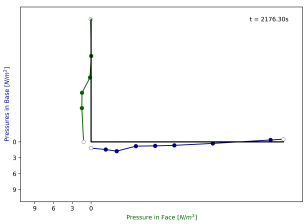

(k) Timestamp: 2176.30s

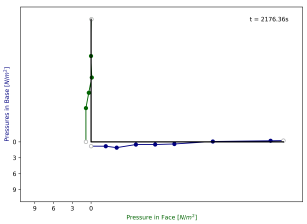

(l) Timestamp: 2176.36s

Figure 46: Individuals stills of pressure distribution along crown wall for the critical wave in a wave spectrum with $H_s = 0.15m$, $s = 2\%$ and $F_c = 0.04m$.

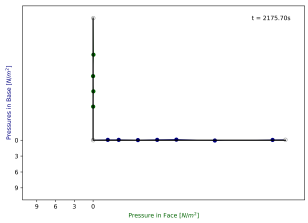

(a) Timestamp: 2175.70s

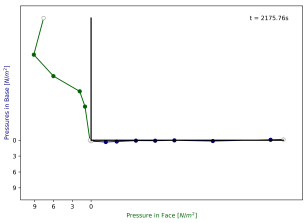

(b) Timestamp: 2175.76s

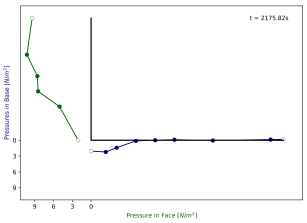

(c) Timestamp: 2175.82s

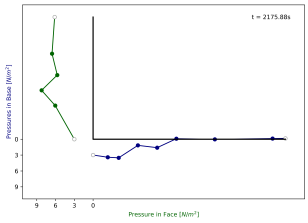

(d) Timestamp: 2175.88s

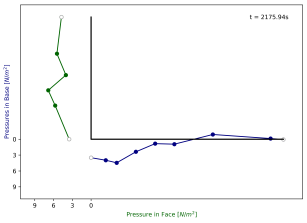

(e) Timestamp: 2175.94s

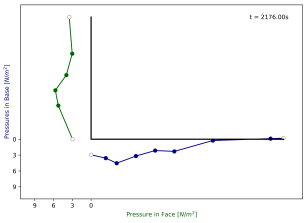

(f) Timestamp: 2176.00s

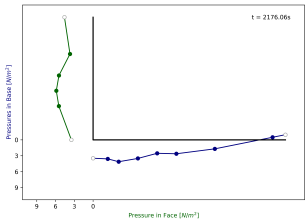

(g) Timestamp: 2176.06s

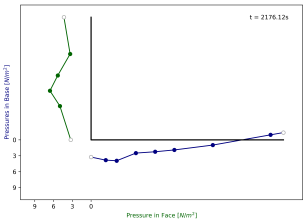

(h) Timestamp: 2176.12s

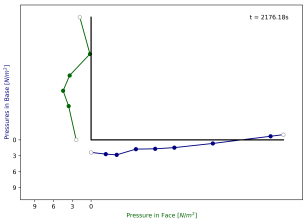

(i) Timestamp: 2176.18s

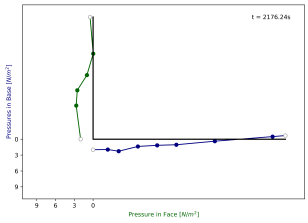

(j) Timestamp: 2176.24s

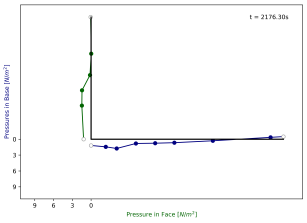

(k) Timestamp: 2176.30s

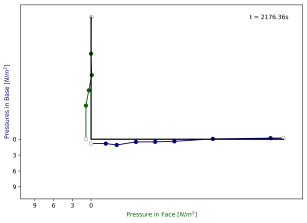

(l) Timestamp: 2176.36s

Figure 47: Individuals stills of pressure distribution along crown wall for the critical wave in a wave spectrum with $H_s = 0.15m$, $s = 2\%$ and $F_c = 0.04m$.